symmetry

MDPI

Article

Operator Spectral Stability Theory and Chebyshev Spectral Collocation Method for Time-Varying Bilateral Quaternion Dynamical Systems

Xiang Si * and Jianwen Zhou *

School of Mathematics and Statistics, Yunnan University, Kunming 650500, China
* Correspondence: devoted_to_study@126.com (X.S.); jwzhou@ynu.edu.cn (J.Z.)

Abstract

This paper develops a structured analytical framework and a robust numerical methodology for the spectral stability of time-varying bilateral quaternion differential equations of the form $\dot{q} = A(t)q + qB(t)$. By systematically extending classical real matrix theory to non-commutative dynamical systems via exact isometric real representations, this study utilizes the Kronecker product of real adjoint matrices to rigorously elucidate the underlying tensor structure of the bilateral evolution operator. This tensor-based reformulation proves that the Floquet multipliers of the bilaterally coupled system can be strictly decoupled into the product of the spectra corresponding to the left and right unilateral subsystems. Second, a "Scalar-Vector Stability Separation Principle" based on logarithmic norms is proposed, demonstrating that the transient energy evolution of the system is governed exclusively by the Hermitian real parts of the coefficient matrices, remaining entirely independent of the anti-Hermitian imaginary parts (rotation terms). Furthermore, for constant-coefficient and slowly varying systems, the Riesz projection from holomorphic functional calculus is introduced to establish algebraic criteria for exponential dichotomies, thereby revealing a cubic scaling law that relates the robustness threshold to the spectral gap ($\varepsilon_0 \propto \beta^3$). Numerically, a Quaternion Chebyshev Spectral Collocation Method (Q-CSCM) is embedded within this exact vectorization framework to ensure that the algebraic symmetries of the bilateral system are strictly preserved through the isomorphic mapping. By explicitly constructing the fully discrete Kronecker product matrix via the exact real vectorization isomorphism, discrete energy estimates are utilized to rigorously prove that the numerical scheme successfully inherits the intrinsic spectral accuracy of the Chebyshev approximation. Comprehensive numerical experiments demonstrate that, within the low-dimensional regime, this methodology exhibits substantial temporal approximation efficiency advantages and superior numerical robustness compared to an alternative Legendre spectral baseline, as well as traditional explicit and state-of-the-art implicit symplectic Runge–Kutta methods, particularly when solving stiff and critically stable problems such as nonlinear Riccati oscillators.

Keywords: quaternion differential equations; bilateral linear systems; floquet theory; spectral collocation method

MSC: 65L60; 34L15; 65P40; 65F15

Check for updates

Academic Editors: Giacomo Capizzi, Rafal Brociek and Mariusz Pleszczyński

Received: 4 March 2026
Revised: 25 March 2026
Accepted: 26 March 2026
Published: 28 March 2026

Copyright: © 2026 by the authors. Licensee MDPI, Basel, Switzerland. This article is an open access article distributed under the terms and conditions of the Creative Commons Attribution (CC BY) license.

1. Introduction

1.1. Research Background and Physical Motivation

Since Hamilton's discovery of Quaternions ($\mathbb{H}$) in 1843, this non-commutative division algebra has transitioned from a purely theoretical algebraic structure into a foundational mathematical language within modern physics and engineering sciences. Unlike the complex field $\mathbb{C}$, the non-commutative nature of quaternion algebra offers unique advantages in describing rotation groups in three- and four-dimensional Euclidean spaces ($SO(3)$ and $SO(4)$) [1], effectively avoiding kinematic singularities such as gimbal lock. Consequently, differential equations defined on quaternion algebras have naturally become the principal descriptive tools for physical models in rigid body attitude dynamics, quantum mechanical spin systems [2], and Euler fluid dynamics.

To appropriately motivate the theoretical framework proposed herein, it is imperative to emphasize its direct applicability to modern physics and engineering. In rigid body attitude dynamics, particularly for asymmetric spacecraft subject to time-varying external torques, the kinematic and dynamic evolution is fundamentally described by quaternion models [1]. As subsequent sections will elucidate, the perturbation analysis of such orientation quaternions naturally yields a bilaterally coupled linear system. Similarly, in quantum mechanical spin systems, the temporal evolution of spin states interacting with non-collinear or time-dependent magnetic fields is governed by quaternion differential equations, where inherent non-commutativity ensures that left and right multiplications characterize fundamentally distinct physical coupling mechanisms [2]. Therefore, establishing a rigorous stability theory for bilateral systems provides essential mathematical tools for predicting critical dynamic behaviors, such as attitude tumbling in aerospace engineering or spin resonance phenomena in quantum mechanics.

In these applications, the quaternion Riccati equation

$$\dot{q}(t) = q(t)a(t)q(t) + b(t)q(t) + q(t)d(t) + c(t), \tag{1}$$

occupies a pivotal position. It not only describes the kinematic evolution of the Frenet frame but is also crucial for feedback gain calculation in optimal control theory. Understanding the asymptotic behavior, periodic orbits, and stability of the solutions to Equation (1) is essential for system design.

In the study of dynamical systems, establishing the existence of periodic orbits is merely a preliminary step; their practical physical significance inherently depends on their local asymptotic stability. To analyze the local asymptotic behavior of a periodic solution $q^*(t)$ of the Riccati equation, one must examine the evolution of its infinitesimal perturbation $\delta q(t) = q(t) - q^*(t)$. Substituting $q(t) = q^*(t) + \delta q(t)$ into Equation (1) and neglecting higher-order terms yields the variational equation:

$$\delta\dot{q}(t) = [q^*(t)a(t) + b(t)]\delta q(t) + \delta q(t)[a(t)q^*(t) + d(t)].$$

Let $A(t) = q^*(t)a(t) + b(t)$ and $B(t) = a(t)q^*(t) + d(t)$, then the above variational equation transforms into a time-varying bilateral linear quaternion differential equation:

$$\dot{q}(t) = A(t)q(t) + q(t)B(t). \tag{2}$$

Equation (2) reveals a critical theoretical challenge: owing to the non-commutativity of quaternion multiplication (i.e., $Aq \neq qA$), the operator mapping $q \mapsto Aq + qB$ cannot be algebraically condensed into a single coefficient matrix multiplication, as is customary in commutative algebras. Consequently, foundational stability theories established for unilateral linear systems ($\dot{q}(t) = A(t)q(t)$) are structurally incompatible with such

bilaterally coupled dynamics. Therefore, establishing an operator spectral stability theory (Floquet Theory) specifically tailored for bilateral linear systems (2), coupled with corresponding high-precision, structure-preserving numerical algorithms, constitutes both a fundamental theoretical requirement for advancing quaternion differential equations and an indispensable prerequisite for determining the stability of nonlinear Riccati equations.

1.2. Literature Review

The analytical theory of quaternion differential equations has attracted widespread attention in mathematical physics and applied mathematics over the past few decades. Existing research results mainly focus on three dimensions: qualitative existence of nonlinear ordinary differential equations, operator analytical theory of elliptic partial differential equations, and fundamental algebraic structures of unilateral linear systems. However, systematic investigations into "time-varying bilateral linear dynamical systems" and their corresponding "high-precision numerical frameworks" remain notably scarce.

1.2.1. Qualitative Analysis of Nonlinear ODEs and Limitations

In the field of ordinary differential equations, the quaternion Riccati equation has received significant attention due to its core status in optimal control and differential geometry. Wilczyński conducted pioneering research on such equations [3,4]. Utilizing the Ważewski topological method and the Brouwer fixed-point theorem, Wilczyński introduced the powerful geometric tool of "periodic isolating segments," rigorously proving the existence of at least two periodic solutions for the Riccati equation under specific coefficient conditions without explicitly constructing the solutions.

Gap 1: While Wilczyński's qualitative and topological approach successfully establishes the existence of periodic solutions, it fundamentally lacks quantitative criteria for determining the linear stability of these orbits. Similarly, Gasull et al. investigated the structure of homogeneous quaternion polynomial differential equations [5], yet there remains a distinct absence of mathematical tools—analogous to classical real-domain Floquet theory—capable of precisely characterizing the convergence rates and stability boundaries surrounding these periodic trajectories.

1.2.2. Operator Methods for PDEs and Limitations

In the fields of partial differential equations (PDEs) and geometric analysis, operator algebra methods have proven to be effective means of handling non-commutative structures. Alesker deeply investigated the quaternion Monge–Ampère equation on compact hypercomplex manifolds, solving the solvability problem of this highly nonlinear equation by establishing refined C^0 and C^2 a priori estimates [6]. On the other hand, Abreu Blaya et al. established a complete operator theory framework for the Cimmino system (a class of first-order linear PDE systems) [7]. They successfully handled elliptic boundary value problems by utilizing the Teodorescu transform and Cauchy-type integral operators in quaternion analysis via a method of matrixifying bilateral operators. In recent years, the analytical framework for quaternion systems has been extensively broadened to address stability and synchronization issues in time-dependent quaternion-valued neural networks [8] and to investigate the Hyers–Ulam stability of linear quaternion-valued differential equations [9].

Gap 2: The aforementioned studies predominantly concentrate on static boundary value problems within spatial domains or geometric structures on manifolds, thereby circumventing the time-evolution operators inherent to dynamical systems. Specifically, while Abreu Blaya et al. successfully introduced operator matrix representations, their methodology was not extended to encompass the semigroup properties and dynamic spectral structures essential for analyzing time-varying ODEs.

1.2.3. Fundamental Theory of Linear Systems and the Limitations of Naive Realification

For the most fundamental linear time-varying systems, existing native theories mainly focus on unilateral systems $\dot{q}(t) = A(t)q(t)$ [10] or specific solvable forms of simple differential equations [11]. Recent studies have established quaternion versions of the Wronskian determinant and Liouville's formula for unilateral systems, clarifying the algebraic characteristics of the solution space as a right free module.

However, for bilateral systems (2) derived from the linearized Riccati equation, unilateral fundamental solution theories fail. Specifically, quaternion non-commutativity ($Aq \neq qA$) prevents the bilateral operator $\mathcal{L}[q] = Aq + qB$ from being algebraically condensed into a single-sided multiplication. Presently, the standard paradigm for addressing such structural challenges is the "realification" approach, which utilizes an isomorphism $\chi : \mathbb{H}^n \to \mathbb{R}^{4n}$ to map the problem into a high-dimensional real system.

Gap 3: Although the realification method is theoretically complete and serves as an indispensable mathematical bridge, directly applying it to bilateral systems without further algebraic refinement presents two inherent challenges: 1. **Structural Obscuration:** Directly analyzing the Floquet multipliers defined via $4n \times 4n$ real matrices obscures the underlying tensor algebraic symmetries of the quaternion operators. Consequently, without incorporating explicit algebraic decomposition, the realification method fails to reveal the intrinsic decoupling relationship between the spectral radius $\rho(\mathcal{M})$ of the overall bilateral system and the independent spectral radii $\rho(\Phi_A), \rho(\Phi_B)$ of the unilateral operators, rendering theoretical analysis computationally cumbersome and devoid of physical intuition. 2. **Curse of Dimensionality in Stability Determination:** From an algorithmic perspective, transforming an n-dimensional quaternion matrix differential equation into a $4n^2$-dimensional real system without exploiting its tensor structure results in a prohibitive increase in computational complexity. Specifically, the complexity of determining the monodromy matrix eigenvalues surges from $\mathcal{O}(n^3)$ to $\mathcal{O}((4n^2)^3) = 64\mathcal{O}(n^6)$, which becomes analytically and computationally intractable when executing parameter continuation or structural bifurcation analyses.

1.2.4. Accuracy Bottlenecks and Benchmarking in Numerical Methods

Within the domain of numerical solutions, contemporary research has achieved significant advancements in structure-preserving algorithms, including geometric integrators and symplectic methods specifically tailored for hypercomplex systems [12,13]. Recently, this momentum has aggressively expanded into structure-preserving numerical linear algebra, producing advanced quaternion iterative solvers such as quaternion generalized minimal residual (QGMRES) methods [14], quaternion biconjugate gradient methods [15], and structure-preserving relaxation iterations [16]. For time-domain integration, state-of-the-art alternatives, such as high-order Gauss–Legendre implicit Runge–Kutta (GL-IRK) schemes, demonstrate exceptional performance in preserving geometric properties within stiff or critically stable dynamic regimes. Nevertheless, numerical algorithms explicitly designed to globally approximate general bilateral quaternion differential equations remain critically underexplored. While foundational techniques like the explicit fourth-order Runge–Kutta (ERK4) scheme can be directly applied to the realified system, they provide an inadequate baseline for rigorously benchmarking highly smooth analytical solutions. Furthermore, even the most sophisticated local symplectic integrators are fundamentally constrained by algebraic accuracy, exhibiting truncation errors that decay strictly proportional to a polynomial power of the step size h (e.g., $\mathcal{O}(h^4)$). Consequently, there is a distinct paucity of high-precision spectral methods tailored for quaternion differential equations; in particular, Chebyshev spectral collocation techniques capable of directly processing bilateral non-commutative terms ($\dot{q} = Aq + qB$) are virtually non-existent. This methodological

deficiency severely impedes the precise resolution of complex dynamical behaviors in quaternion systems, such as orbital dynamics at the edge of chaos or the detection of extremely weak instabilities.

In summary, while existing literature has substantially advanced the qualitative topology of Riccati equations, operator frameworks for PDEs, and the algebraic foundations of unilateral linear systems, a systematic "tensor-based reformulation framework for bilateral time-varying linear systems"—which successfully translates non-commutative dynamics into tractable real-valued spectral problems, integrated with a structure-preserving, high-precision numerical framework—remains critically absent. Addressing this methodological void constitutes the primary objective of this paper.

1.3. Main Contributions

Addressing the aforementioned challenges, this paper aims to establish a complete operator spectral theory for time-varying bilateral quaternion dynamical systems and, on this basis, propose a high-precision structure-preserving spectral collocation algorithm (Q-CSCM). The main contributions of this paper are summarized as follows:

1. **Tensor-based reformulation of bilateral evolution operators.** This paper systematically extends classical real matrix theory to non-commutative domains by deeply exploiting the exact real vectorization isomorphism. Specifically, the Kronecker product is utilized to reformulate and reveal the underlying tensor structure of bilateral evolution operators. This formulation rigorously proves that the Floquet multipliers of a bilateral system can be strictly decoupled into the product of the single-valued matrix spectra associated with the left and right unilateral subsystems (Theorem 4). This analytical reduction decreases the complexity of stability determination from $\mathcal{O}(n^6)$ down to $2 \times \mathcal{O}(n^3)$.

2. **Proposal of the "Scalar-Vector Stability Separation Principle" and "Riesz Projection Characterization".** For general time-varying systems, logarithmic norm theory is applied to prove that the instantaneous energy growth of the system is governed solely by the Hermitian real parts of the coefficient matrices, remaining strictly independent of the anti-Hermitian imaginary parts representing rotation (Theorem 5). Furthermore, for constant-coefficient and slowly varying systems, the Riesz projection from holomorphic functional calculus is introduced to explicitly construct projection operators for stable and unstable subspaces (Theorem 6), thereby deriving a robustness boundary $\varepsilon_0 \propto \beta^3$ for exponential dichotomies under slowly varying conditions (Theorem 7).

3. **Integration of Q-CSCM within a structure-preserving isomorphic framework.** By strictly embedding the standard Chebyshev spectral approximation into this exactly vectorized real linear system, the structural fidelity of the numerical scheme is completely endowed by the exact real isomorphic mapping. The resulting architecture achieves highly accurate spectral discretization while intrinsically inheriting the underlying 4×4 block symplectic symmetries of the quaternion operator algebras. Through discrete energy estimates, the algorithm is mathematically proven to achieve spectral accuracy convergence. Comprehensive numerical experiments demonstrate that, within the low-dimensional regime, this methodology exhibits substantial temporal approximation efficiency advantages and superior numerical robustness compared to an alternative Legendre Spectral Collocation Method (Q-LSCM) baseline, as well as both traditional explicit RK4 and state-of-the-art implicit symplectic GL-IRK4 methods, specifically when resolving stiff, multi-frequency, and critically stable oscillatory problems.

1.4. Paper Structure

The structure of this paper is arranged as follows: Section 2 introduces the foundations of quaternion algebra and vectorization; Section 3 establishes the operator spectral theory

for bilateral systems, including Floquet decoupling, scalar-vector separation, and Riesz projection theory; Section 4 details the construction and convergence analysis of the Q-CSCM algorithm; Section 5 verifies the effectiveness of the theory and algorithm through numerical experiments; and Section 6 concludes the paper.

2. Preliminaries

2.1. Foundations of Quaternion Algebra

The real quaternion algebra $\mathbb{H}$ is a four-dimensional vector space over the real field $\mathbb{R}$, with the standard basis e_0, e_1, e_2, e_3 (commonly denoted as $1, \mathbf{i}, \mathbf{j}, \mathbf{k}$). Any quaternion $q \in \mathbb{H}$ can be uniquely represented as

$$q = q_0 + q_1\mathbf{i} + q_2\mathbf{j} + q_3\mathbf{k}, \quad q_m \in \mathbb{R}, m = 0, 1, 2, 3.$$

According to Hamilton's rules, the multiplication of basis elements satisfies non-commutativity and associativity:

$$\mathbf{i}^2 = \mathbf{j}^2 = \mathbf{k}^2 = \mathbf{ijk} = -1, \ \mathbf{ij} = -\mathbf{ji} = \mathbf{k}, \ \mathbf{jk} = -\mathbf{kj} = \mathbf{i}, \ \mathbf{ki} = -\mathbf{ik} = \mathbf{j}.$$

The $\mathbb{H}$ defined in this way constitutes a normed non-commutative division ring or skew field.

For a quaternion q, we call q_0 the scalar part, denoted as $\mathrm{Re}(q)$, and $q_1\mathbf{i} + q_2\mathbf{j} + q_3\mathbf{k}$ the vector part, denoted as $\mathrm{Im}(q)$. The conjugate of a quaternion is defined as an involutive automorphism:

$$\bar{q} = \mathrm{Re}(q) - \mathrm{Im}(q) = q_0 - q_1\mathbf{i} - q_2\mathbf{j} - q_3\mathbf{k}.$$

The modulus or norm of a quaternion is defined as

$$|q| = \sqrt{q\bar{q}} = \sqrt{\bar{q}q} = \sqrt{q_0^2 + q_1^2 + q_2^2 + q_3^2}.$$

The modulus possesses the extremely important property of multiplicative homomorphism, i.e., for any $p, q \in \mathbb{H}$:

$$|pq| = |p||q|. \tag{3}$$

This property will play a core role in proving the spectral radius decoupling of bilateral operators in Theorem 4. The inverse of a non-zero quaternion q exists and is unique, given by $q^{-1} = \bar{q}/|q|^2$.

For time-varying systems, consider continuously differentiable functions $q(t)$ mapping a real interval $\mathcal{I} \subset \mathbb{R}$ to $\mathbb{H}$. Because quaternion multiplication is non-commutative, the product rule for differentiation must strictly preserve the order of multiplication. Let $p(t), q(t)$ be quaternion-valued differentiable functions, then

$$\frac{d}{dt}(p(t)q(t)) = \dot{p}(t)q(t) + p(t)\dot{q}(t). \tag{4}$$

It is precisely because $\dot{p}q \neq q\dot{p}$ that when linearizing the Riccati equation, terms of the form $A(t)q(t) + q(t)B(t)$ cannot be merged, thus mathematically necessitating the concept of bilateral linear systems.

Developing high-precision numerical algorithms requires transforming quaternion operators into computationally tractable algebraic forms, which necessitates the introduction of real matrix representations. For any $q \in \mathbb{H}$, we define the isomorphism $\chi_L : \mathbb{H} \to \mathbb{R}^{4\times4}$ as the matrix representation of its left multiplication operator $L_q(x) = qx$ [17], and

simultaneously define $\chi_R : \mathbb{H} \to \mathbb{R}^{4\times4}$ as the matrix representation of its right multiplication operator $R_q(x) = xq$:

$$\chi_L(q) = \begin{pmatrix} q_0 & -q_1 & -q_2 & -q_3 \\ q_1 & q_0 & -q_3 & q_2 \\ q_2 & q_3 & q_0 & -q_1 \\ q_3 & -q_2 & q_1 & q_0 \end{pmatrix}, \quad \chi_R(q) = \begin{pmatrix} q_0 & -q_1 & -q_2 & -q_3 \\ q_1 & q_0 & q_3 & -q_2 \\ q_2 & -q_3 & q_0 & q_1 \\ q_3 & q_2 & -q_1 & q_0 \end{pmatrix} \tag{5}$$

These two matrix representations possess the following key algebraic properties, which form the basis of the operator spectral analysis in Section 3:

1. **Algebraic Homomorphism and Anti-homomorphism:** Left multiplication satisfies the homomorphism property $\chi_L(pq) = \chi_L(p)\chi_L(q)$, while right multiplication satisfies the anti-homomorphism property $\chi_R(pq) = \chi_R(q)\chi_R(p)$.
2. **Left-Right Commutativity:** The left multiplication operator and the right multiplication operator commute (corresponding to the associativity of quaternions $(pq)r = p(qr)$). That is, for any $p, q \in \mathbb{H}$, their real matrix representations satisfy

$$\chi_L(p)\chi_R(q) = \chi_R(q)\chi_L(p). \tag{6}$$

3. **Trace Property:** The relationship between the real part of a quaternion and the trace of the matrix is

$$\mathrm{Tr}(\chi_L(q)) = \mathrm{Tr}(\chi_R(q)) = 4\mathrm{Re}(q).$$

2.2. Spectral Properties of Quaternion Matrices

Let $M_n(\mathbb{H})$ denote the set of all $n \times n$ quaternion matrices. For $A \in M_n(\mathbb{H})$, due to the non-commutativity of scalar multiplication, one must distinguish between left eigenvalues [18] and right eigenvalues. In the theory of quaternion linear differential equations, the solution space is typically endowed with a right $\mathbb{H}$-module structure. To remain compatible with this geometric structure, this paper uniformly adopts the definition of right eigenvalues [19].

Definition 1. *If there exists $\lambda \in \mathbb{H}$ and a non-zero vector $x \in \mathbb{H}^n$ such that*

$$Ax = x\lambda,$$

then λ is called a right eigenvalue of matrix A, and x is called the corresponding right eigenvector. The set of all right eigenvalues of A is called the right spectrum, denoted as $\sigma_r(A)$.

Unlike real or complex matrices, the spectrum of a quaternion matrix has a unique geometric structure. If λ is a right eigenvalue of A and $Ax = x\lambda$, then for any non-zero quaternion $u \in \mathbb{H}$, consider the vector $y = xu$:

$$Ay = A(xu) = (Ax)u = (x\lambda)u = (xu)(u^{-1}\lambda u) = y(u^{-1}\lambda u).$$

This implies that if $\lambda \in \sigma_r(A)$, then all elements in its entire conjugacy class, denoted by $[\lambda] = \{u^{-1}\lambda u \mid u \in \mathbb{H}, u \neq 0\}$, are also right eigenvalues of A.

For a non-real quaternion λ, its conjugacy class $[\lambda]$ geometrically constitutes a 2-sphere in $\mathbb{R}^4$ space. However, according to the multiplicative property of the modulus in Formula (3), the conjugate transformation preserves the modulus:

$$|u^{-1}\lambda u| = |u|^{-1}|\lambda||u| = |\lambda|.$$

This property is fundamental, indicating that while eigenvalues vary across the conjugacy sphere, their modulus $|\lambda|$ remains the unique intrinsic invariant of the conjugacy class $[\lambda]$.

Based on this, we can rigorously define the spectral radius of a quaternion matrix as the core metric for subsequent Floquet stability analysis:

$$\rho(A) = \sup\{|\lambda| : \lambda \in \sigma_r(A)\}. \tag{7}$$

Note that while the right spectrum $\sigma_r(A)$ consists of entire conjugacy classes $[\lambda]$, the real representation matrix $\chi_L(A) \in M_{4n}(\mathbb{R})$ possesses a discrete set of complex eigenvalues. There is an essential connection between these structures: for each conjugacy class $[\lambda] \subset \sigma_r(A)$, the complex eigenvalues of $\chi_L(A)$ contain the complex representatives (and their conjugates) of that class. Consequently, although the individual eigenvalues differ in nature, their moduli coincide perfectly. Therefore, the set of eigenvalue moduli of $\chi_L(A)$ is entirely identical to the set of right eigenvalue moduli of A. This yields the following equivalent calculation formula:

$$\rho(A) = \max\{|\mu| : \mu \in \sigma(\chi_L(A))\}.$$

Consequently, the spectral radius of the quaternion matrix A can be exactly determined by computing the spectral radius (i.e., the eigenvalue with the maximum modulus) of the corresponding $4n \times 4n$ real matrix $\chi_L(A)$, which is pivotal for assessing system stability.

2.3. Operator Vectorization and Real Representation

The primary difficulty in analyzing the bilateral linear differential equation $\dot{Q} = A(t)Q + Q(t)B(t)$ arises because the operator $\mathcal{L}_{A,B}[Q] = AQ + QB$ cannot be algebraically condensed within the quaternion algebra $\mathbb{H}$. Overcoming this obstacle and constructing numerical algorithms requires employing real vector space isomorphisms to "vectorize" the quaternion operator.

Let $M_{n\times m}(\mathbb{H})$ be the $n \times m$ dimensional quaternion matrix space. For any $Q \in M_{n\times m}(\mathbb{H})$, we define the real vectorization operator $\nu : M_{n\times m}(\mathbb{H}) \to \mathbb{R}^{4nm}$. This operator first expands each column vector $Q_{\cdot j}$ of Q, then uses the scalar isomorphism $\mathbb{H} \cong \mathbb{R}^4$ preceding Equation (5) to transform each element into a 4-dimensional real column vector, and finally stacks them column-wise to form a $4nm$-dimensional real vector. Formally, the operator ν constructs an isometric real linear isomorphism between the quaternion matrix space $M_{n\times m}(\mathbb{H})$ (viewed as a $4nm$-dimensional vector space over $\mathbb{R}$) and the Euclidean space $\mathbb{R}^{4nm}$. This isomorphism preserves the linear structure and norm properties of the space, thereby ensuring that the asymptotic stability of the original quaternion dynamical system is completely equivalent to that of the transformed real dynamical system.

Based on the left and right multiplication real representation matrices χ_L, χ_R defined in Section 2.1, we can construct the full real representation of quaternion matrices. For $A = (a_{ij}) \in M_n(\mathbb{H})$, define its left real adjoint matrix $\mathbf{A}_L \in M_{4n}(\mathbb{R})$ as the following block matrix:

$$\mathbf{A}_L = \begin{pmatrix} \chi_L(a_{11}) & \chi_L(a_{12}) & \cdots & \chi_L(a_{1n}) \\ \chi_L(a_{21}) & \chi_L(a_{22}) & \cdots & \chi_L(a_{2n}) \\ \vdots & \vdots & \ddots & \vdots \\ \chi_L(a_{n1}) & \chi_L(a_{n2}) & \cdots & \chi_L(a_{nn}) \end{pmatrix}. \tag{8}$$

Similarly, define its right real adjoint matrix $\mathbf{A}_R \in M_{4n}(\mathbb{R})$:

$$\mathbf{A}_R = \begin{pmatrix} \chi_R(a_{11}) & \chi_R(a_{12}) & \cdots & \chi_R(a_{1n}) \\ \chi_R(a_{21}) & \chi_R(a_{22}) & \cdots & \chi_R(a_{2n}) \\ \vdots & \vdots & \ddots & \vdots \\ \chi_R(a_{n1}) & \chi_R(a_{n2}) & \cdots & \chi_R(a_{nn}) \end{pmatrix}. \tag{9}$$

Using the above definitions, we can establish the following key algebraic identities, transforming quaternion matrix multiplication into real matrix-vector multiplication:

Lemma 1. *For any $A \in M_n(\mathbb{H})$, $B \in M_m(\mathbb{H})$, and $Q \in M_{n\times m}(\mathbb{H})$, the following relationships hold:*

1. *Left multiplication vectorization: $\nu(AQ) = (I_m \otimes \mathbf{A}_L)\nu(Q)$;*
2. *Right multiplication vectorization: $\nu(QB) = (\mathbf{B}_R^\top \otimes I_n)\nu(Q)$.*

where $\otimes$ denotes the Kronecker product of real matrices, and I_k designates the $4k \times 4k$ real identity matrix to ensure dimensional consistency within the expanded representation space.

Proof. For left multiplication $Y = AQ$, its j-th column satisfies $Y_{\cdot j} = AQ_{\cdot j}$. Applying the block definition of $\mathbf{A}_L$, we know $\nu(Y_{\cdot j}) = \mathbf{A}_L\nu(Q_{\cdot j})$. Stacking all columns yields the $I_m \otimes \mathbf{A}_L$ structure. For right multiplication $Z = QB$, considering the non-commutativity of quaternion right multiplication and the anti-homomorphism property of χ_R, combined with the properties of matrix transposition in the Kronecker product, the form $\mathbf{B}_R^\top$ can be derived. Here, the principle of commutativity of left and right multiplication operators in Equation (6) is utilized at the matrix level. □

Based on Lemma 1, we can explicitly write the real matrix representation $\mathbf{M}_\mathcal{L} \in M_{4nm}(\mathbb{R})$ of the bilateral linear operator $\mathcal{L}_{A,B}[Q] = AQ + QB$:

$$\mathbf{M}_\mathcal{L} = I_m \otimes \mathbf{A}_L + \mathbf{B}_R^\top \otimes I_n. \tag{10}$$

This formulation is central to the proposed framework. It elucidates the algebraic structure of the bilateral operator under real isomorphism and, crucially, demonstrates that the spectrum of the composite operator $\mathcal{L}_{A,B}$ can be determined by analyzing the sum of the individual spectra of $\mathbf{A}_L$ and $\mathbf{B}_R$. This provides a rigorous algebraic foundation for decoupling the stability analysis of bilateral systems using unilateral spectral information in Section 3.

3. Operator Spectral Stability of Bilateral Linear Systems

This section is dedicated to developing a structured analytical framework for time-varying bilateral linear quaternion differential equations. Unlike the Floquet theory established by Kou and Xia [10] for unilateral systems, we systematically utilize the real adjoint matrix framework introduced by Zhang [17] as a rigorous algebraic bridge. By mapping the bilateral operators into an augmented real tensor space, this exact isomorphism facilitates a systematic reformulation of the non-commutative dynamics into a mathematically tractable real-valued system. Through this tensor product structure, the bilateral evolution operators are rigorously characterized, enabling the establishment of spectral decoupling properties by leveraging the trace and spectrum of the corresponding real matrix representations.

3.1. Definition and Tensor Product Structure of Bilateral Evolution Operators

Prior to establishing the spectral stability theory, it is necessary to rigorously define the existence, uniqueness, and algebraic evolution mechanisms of solutions for bilateral linear

systems within a general Banach space framework. Consider the homogeneous bilateral time-varying linear system defined on the n-dimensional quaternion vector space $\mathbb{H}^n$:

$$\dot{q}(t) = \mathcal{L}(t)[q(t)] \triangleq A(t)q(t) + q(t)B(t), \quad t \in \mathcal{I}. \tag{11}$$

where $\mathcal{I} \subseteq \mathbb{R}$ is a real interval containing the initial time t_0, and $q(t) \in \mathbb{H}^n$ is the system state vector. We assume that the coefficient matrix functions $A(\cdot), B(\cdot) : \mathcal{I} \to M_n(\mathbb{H})$ are continuous on the interval $\mathcal{I}$.

3.1.1. Operator-Theoretic Definition of Bilateral Evolution Operators

Although the non-commutativity of quaternion multiplication prevents the mapping $\mathcal{L}(t) : q \mapsto Aq + qB$ from being simplified into a single matrix multiplication, it remains a well-defined bounded linear operator acting on $\mathbb{H}^n$. The temporal evolution of the system state is thus formally described by introducing the bilateral evolution operator.

Definition 2. *Let $\mathcal{B}(\mathbb{H}^n)$ be the Banach space of bounded linear operators on $\mathbb{H}^n$. A two-parameter family of operators $\mathcal{U}(t, t_0) : \mathbb{H}^n \to \mathbb{H}^n (t, t_0 \in \mathcal{I})$ is called the bilateral evolution operator for system (11) if it satisfies the following axioms:*

- ***Differentiation Property:*** *For any fixed initial vector $w \in \mathbb{H}^n$, the map $t \mapsto \mathcal{U}(t, t_0)[w]$ is continuously differentiable on $\mathcal{I}$ and satisfies Equation (11) pointwise:*

$$\frac{\partial}{\partial t}\mathcal{U}(t, t_0)[w] = A(t)(\mathcal{U}(t, t_0)[w]) + (\mathcal{U}(t, t_0)[w])B(t).$$

- ***Identity Property:*** *$\mathcal{U}(t_0, t_0) = \mathcal{I}_{\mathbb{H}^n}$, where $\mathcal{I}_{\mathbb{H}^n}$ is the identity operator.*
- ***Semigroup Property:*** *For any $t, s, t_0 \in \mathcal{I}$, the evolution operator satisfies the composition law:*

$$\mathcal{U}(t, s) \circ \mathcal{U}(s, t_0) = \mathcal{U}(t, t_0).$$

3.1.2. Tensor Structure Theorem of Evolution Operators

Although system (11) is defined on a non-commutative algebra, via the real vectorization isomorphism $\nu : \mathbb{H}^n \to \mathbb{R}^{4n}$ introduced in Section 2.3, the system is topologically and differentially equivalent to a real linear system on $\mathbb{R}^{4n}$:

$$\dot{\mathbf{x}} = \mathbf{M}_{\mathcal{L}}(t)\mathbf{x}.$$

Since the continuity of $A(t), B(t)$ guarantees the continuity of their real representation matrix $\mathbf{M}_{\mathcal{L}}(t)$, according to the Picard–Lindelöf theorem in classical ordinary differential equation theory, the solution operator for this real system exists and is unique. By the invertibility of the isomorphism ν, the solution operator $\mathcal{U}(t, t_0)$ for the quaternion bilateral system also exists and is unique.

The following theorem is the core result of this section. It not only provides an explicit construction of $\mathcal{U}(t, t_0)$ but also reveals that the dynamics of the bilateral system can be decoupled into the tensor product of left-side evolution and right-side evolution. This structural property is the physical basis for deriving the spectral radius decoupling formula (Theorem 4).

Theorem 1. *Let $\Phi_A(t, t_0) \in M_n(\mathbb{H})$ be the normalized left fundamental solution matrix of the left subsystem $\dot{U} = A(t)U$ (satisfying $\Phi_A(t_0, t_0) = I_n$); let $\Phi_B(t, t_0) \in M_n(\mathbb{H})$ be the normalized right fundamental solution matrix of the right subsystem $\dot{V} = VB(t)$ (satisfying $\Phi_B(t_0, t_0) = I_n$). Then, the unique evolution operator $\mathcal{U}(t, t_0)$ of the bilateral linear system (11) has the following form of explicit separation of variables: For any initial state $X \in \mathbb{H}^n$ (or generalized to matrix initial value $X \in M_{n\times m}(\mathbb{H})$),*

$$q(t) = \mathcal{U}(t, t_0)[X] = \Phi_A(t, t_0) \cdot X \cdot \Phi_B(t, t_0). \tag{12}$$

Proof. The proof proceeds in three stages: verifying that the constructed form satisfies the governing differential equation, validating the initial condition, and confirming uniqueness via the Picard–Lindelöf theorem. To simplify notation, the parameters (t, t_0) are omitted below, and we denote $\Phi_A \equiv \Phi_A(t, t_0)$ and $\Phi_B \equiv \Phi_B(t, t_0)$. We need to verify whether the constructed solution $q(t) = \Phi_A X \Phi_B$ satisfies the original equation $\dot{q} = Aq + qB$. Differentiating $q(t)$ with respect to time t and noting that quaternion multiplication does not satisfy commutativity, we apply the product rule while strictly maintaining the multiplication order. Noting that the initial state X is constant (i.e., $\dot{X} = 0$), we have

$$\dot{q}(t) = \frac{d}{dt}(\Phi_A X \Phi_B) = \dot{\Phi}_A X \Phi_B + \Phi_A X \dot{\Phi}_B, \tag{13}$$

According to the definition of fundamental solution matrices, Φ_A and Φ_B satisfy the following differential equations respectively:

$$\begin{cases} \dot{\Phi}_A(t, t_0) = A(t)\Phi_A(t, t_0), \\ \dot{\Phi}_B(t, t_0) = \Phi_B(t, t_0)B(t). \end{cases}$$

Substituting these two differential relations into Equation (13), and using the associativity of matrix multiplication, we obtain

$$\begin{aligned} \dot{q}(t) &= (A(t)\Phi_A)X\Phi_B + \Phi_A X(\Phi_B B(t)) \\ &= A(t)(\Phi_A X \Phi_B) + (\Phi_A X \Phi_B)B(t) \\ &= A(t)q(t) + q(t)B(t). \end{aligned}$$

Thus, the constructed form (12) indeed satisfies the bilateral differential Equation (11). Furthermore, when $t = t_0$, using the normalization property of fundamental solution matrices $\Phi_A(t_0, t_0) = I_n$ and $\Phi_B(t_0, t_0) = I_n$, we have

$$\mathcal{U}(t_0, t_0)[X] = I_n \cdot X \cdot I_n = X.$$

This indicates that the operator satisfies the identity axiom. At the same time, system (11) is equivalent under real isomorphism to a linear ordinary differential equation on the Banach space $\mathbb{R}^{4n}$. Since the coefficient matrices $A(t)$ and $B(t)$ are continuous on interval $\mathcal{I}$, according to the Picard–Lindelöf uniqueness theorem, the solution passing through initial value X is unique. Therefore, Equation (12) is not just a special case of a solution, but the unique expression of the evolution operator $\mathcal{U}(t, t_0)$. □

3.2. Generalized Liouville Formula

In classical theory, Liouville's formula describes the evolution of the determinant (Wronskian) of the fundamental solution matrix. For bilateral systems, since the structure of the solution is no longer simple matrix multiplication, we need to examine the volume expansion rate of the evolution operator $\mathcal{U}(t, t_0)$ in phase space. To maintain theoretical generality, this section considers differential equations defined on the quaternion matrix space $M_n(\mathbb{H})$ (covering the scalar case $n = 1$):

$$\dot{Q}(t) = \mathcal{L}(t)[Q(t)] \triangleq A(t)Q(t) + Q(t)B(t), \quad Q(t_0) = I_n. \tag{14}$$

Definition of Generalized Wronskian

Due to quaternion non-commutativity, directly defining the "determinant" of a quaternion operator is ambiguous. We must define it via real isomorphism. Using the vectorization operator $\nu : M_n(\mathbb{H}) \to \mathbb{R}^{4n^2}$ defined in Section 2.3, the operator Equation (14) is equivalent to a real linear system on $\mathbb{R}^{4n^2}$:

$$\dot{\mathbf{x}}(t) = \mathbf{M}_{\mathcal{L}}(t)\mathbf{x}(t), \quad \mathbf{x} \in \mathbb{R}^{4n^2},$$

where $\mathbf{M}_{\mathcal{L}}(t) \in M_{4n^2}(\mathbb{R})$ is the full real matrix representation of the bilateral operator $\mathcal{L}(t)$. Let $\mathbf{\Phi}_{\mathbb{R}}(t, t_0)$ be the fundamental solution matrix of this real linear system.

Definition 3. *The generalized Wronskian $W(t)$ of the bilateral system (14) is the determinant of the real matrix corresponding to its evolution operator:*

$$W(t) \triangleq \det(\mathbf{\Phi}_{\mathbb{R}}(t, t_0)).$$

According to classical real ODE theory: $\dot{W}/W = \mathrm{Tr}(\mathbf{M}_{\mathcal{L}}(t))$. Therefore, the core of the problem transforms into calculating the trace of the $4n^2 \times 4n^2$ dimensional real matrix $\mathbf{M}_{\mathcal{L}}(t)$.

Theorem 2. *Let $A(t), B(t) \in M_n(\mathbb{H})$ be continuous matrix functions. Then the generalized Wronskian $W(t)$ of system (14) satisfies the following exponential evolution law:*

$$W(t) = W(t_0) \exp\left(\int_{t_0}^{t} 4n \cdot Re[Tr(A(\tau)) + Tr(B(\tau))] d\tau \right). \tag{15}$$

Proof. According to the vectorization identity in Lemma 1, and $\mathrm{Tr}(X+Y) = \mathrm{Tr}(X) + \mathrm{Tr}(Y)$, $\mathrm{Tr}(X \otimes Y) = \mathrm{Tr}(X)\mathrm{Tr}(Y)$, we have

$$\begin{aligned} \mathrm{Tr}(\mathbf{M}_{\mathcal{L}}) &= \mathrm{Tr}(I_n \otimes \mathbf{A}_L) + \mathrm{Tr}(\mathbf{B}_R^{\top} \otimes I_n) \\ &= \mathrm{Tr}(I_n) \cdot \mathrm{Tr}(\mathbf{A}_L) + \mathrm{Tr}(\mathbf{B}_R^{\top}) \cdot \mathrm{Tr}(I_n). \end{aligned}$$

Also, the trace of the real adjoint of a quaternion matrix satisfies $\mathrm{Tr}(\mathbf{A}_L) = 4\mathrm{Re}(\mathrm{Tr}(A))$. Similarly, for $\mathbf{B}_R^{\top}$, we have $\mathrm{Tr}(\mathbf{B}_R^{\top}) = \mathrm{Tr}(\mathbf{B}_R) = 4\mathrm{Re}(\mathrm{Tr}(B))$. Substituting these yields

$$\mathrm{Tr}(\mathbf{M}_{\mathcal{L}}) = 4n[\mathrm{Re}(\mathrm{Tr}(A)) + \mathrm{Re}(\mathrm{Tr}(B))].$$

Then, integrating $\dot{W}/W = \mathrm{Tr}(\mathbf{M}_{\mathcal{L}})$ yields Formula (15). □

3.3. Bilateral Floquet Theory and Spectral Decoupling

In the previous two sections, we established the tensor structure and volume evolution law of the evolution operator. This section will establish a spectral theoretical framework for determining the asymptotic stability of the zero solution for periodic systems. In this section, assume that the coefficient matrices $A(t)$ and $B(t)$ of system (14) are continuous T-periodic functions, i.e., for any $t \in \mathbb{R}$, satisfying

$$A(t+T) = A(t), \quad B(t+T) = B(t).$$

3.3.1. Bilateral Monodromy Operator

According to classical Floquet theory, the stability of a linear periodic system is completely determined by the "state transition operator" at the end of one period. For bilateral systems, this transition is no longer simple matrix multiplication but a linear operator defined on $\mathbb{H}^n$.

Definition 4. *Define the bilateral monodromy operator $\mathcal{M} : \mathbb{H}^n \to \mathbb{H}^n$ as the evolution operator of system (14) over one complete period T: $\mathcal{M} \triangleq \mathcal{U}(T,0)$. According to the tensor structure established in Theorem 1, the action of this operator on any initial vector $X \in \mathbb{H}^n$ has the following explicit form:*

$$\mathcal{M}[X] = M_A X M_B,$$

where: $M_A = \Phi_A(T,0) \in M_n(\mathbb{H})$ is the monodromy matrix of the left subsystem $\dot{U} = A(t)U$; $M_B = \Phi_B(T,0) \in M_n(\mathbb{H})$ is the monodromy matrix of the right subsystem $\dot{V} = VB(t)$.

3.3.2. Stability Criterion

Determining the stability of the system requires analyzing the spectral properties of the operator $\mathcal{M}$. Using the concept of generalized spectral radius defined in Section 2.2, we establish the following stability criterion.

Theorem 3. *The zero solution of the time-varying bilateral linear periodic system (14) is asymptotically stable if and only if the generalized spectral radius of the bilateral monodromy operator $\mathcal{M}$ is strictly less than 1, i.e., $\rho(\mathcal{M}) < 1$. If $\rho(\mathcal{M}) > 1$, the system is unstable.*

Proof. Using the vectorization isomorphism ν, the dynamic behavior of operator $\mathcal{M}$ on the Banach space $\mathbb{H}^n$ is equivalent to the dynamic behavior of the real matrix $\mathbf{M}_{\mathcal{M}}$ on $\mathbb{R}^{4n^2}$. According to classical real Floquet theory, the necessary and sufficient condition for the asymptotic stability of the discrete dynamical system $\mathbf{x}_{k+1} = \mathbf{M}_{\mathcal{M}}\mathbf{x}_k$ is that the moduli of all eigenvalues of $\mathbf{M}_{\mathcal{M}}$ are less than 1. Since the generalized spectral radius $\rho(\mathcal{M})$ of operator $\mathcal{M}$ equals the spectral radius of its equivalent real matrix, the theorem is proven. □

3.3.3. Spectral Decoupling Theorem

Directly calculating the spectral radius of operator $\mathcal{M}$ typically requires constructing and computing the eigenvalues of a $4n^2 \times 4n^2$ real matrix, which is computationally expensive and obscures the physical structure of the bilateral system. The following theorem reveals the separability of the spectral structure, proving that the stability of the bilateral system can be strictly decomposed into the product of its left and right unilateral dynamics.

It is crucial to emphasize that this exact spectral decoupling is not a trivial consequence of tensor algebra, but depends critically on the associativity of the quaternion division ring. Mathematically, this associativity translates to the exact commutativity of the left and right multiplication operators (as established in Equation (6), $L_A \circ R_B = R_B \circ L_A$). Without this fundamental commutativity between the left and right operators, the tensor separation of the monodromy matrix would be algebraically invalid.

Theorem 4. *Let $M_A, M_B \in M_n(\mathbb{H})$ be the monodromy matrices of the left and right subsystems, respectively. Then the generalized spectral radius $\rho(\mathcal{M})$ of the bilateral monodromy operator $\mathcal{M}[X] = M_A X M_B$ satisfies the following exact decoupling relationship:*

$$\rho(\mathcal{M}) = \rho(M_A) \cdot \rho(M_B), \tag{16}$$

where $\rho(M_A)$ and $\rho(M_B)$ are the right eigenvalue spectral radii of the quaternion matrices M_A and M_B, respectively.

Proof. For any $X \in \mathbb{H}^n$, the real vectorization of the operator action $\mathcal{M}[X]$ is given by

$$\nu(\mathcal{M}[X]) = \nu(M_A X M_B).$$

Let $Y = XM_B$. Applying Lemma 1 to the left multiplication yields

$$\nu(M_A Y) = (I_n \otimes (\mathbf{M}_A)_L)\nu(Y).$$

Similarly, for the right multiplication, we have

$$\nu(Y) = \nu(XM_B) = ((\mathbf{M}_B)_R^\top \otimes I_n)\nu(X).$$

Combining the above two equations, the full real matrix representation of the operator $\mathcal{M}$ is obtained as follows:

$$\mathbf{M}_\mathcal{M} = (I_n \otimes (\mathbf{M}_A)_L)((\mathbf{M}_B)_R^\top \otimes I_n).$$

At this juncture, the commutativity of the left and right real representations (inherited from quaternion associativity) guarantees that the tensor factors operate on independent subspaces. Applying the mixed-product property of the Kronecker product, $(A \otimes B)(C \otimes D) = (AC) \otimes (BD)$, we have

$$\mathbf{M}_\mathcal{M} = (I_n \cdot (\mathbf{M}_B)_R^\top) \otimes ((\mathbf{M}_A)_L \cdot I_n) = (\mathbf{M}_B)_R^\top \otimes (\mathbf{M}_A)_L.$$

By the spectral properties of the Kronecker product, the spectrum of $\mathbf{M}_\mathcal{M}$ is

$$\sigma(\mathbf{M}_\mathcal{M}) = \{\mu \cdot \lambda \mid \mu \in \sigma((\mathbf{M}_B)_R^\top), \lambda \in \sigma((\mathbf{M}_A)_L)\}.$$

Consequently, the spectral radius of the operator $\mathcal{M}$, defined as the maximum modulus of the eigenvalues of $\mathbf{M}_\mathcal{M}$, is

$$\begin{aligned}\rho(\mathcal{M}) &= \max\{|\mu\lambda| : \mu \in \sigma((\mathbf{M}_B)_R^\top), \lambda \in \sigma((\mathbf{M}_A)_L)\} \\ &= \max\{|\mu|\} \cdot \max\{|\lambda|\} \\ &= \rho((\mathbf{M}_B)_R^\top) \cdot \rho((\mathbf{M}_A)_L).\end{aligned}$$

Noting the trace and spectral invariances, we obtain

$$\rho((\mathbf{M}_B)_R^\top) = \rho((\mathbf{M}_B)_R) = \rho(M_B), \quad \rho((\mathbf{M}_A)_L) = \rho(M_A).$$

Substituting these identities back into the previous equation completes the proof. □

3.3.4. Physical Significance and Corollary

Theorem 4 indicates that the stability of a bilateral system is determined by the "product" of the stabilities of the left and right subsystems.

Corollary 1. *System* (14) *is asymptotically stable if and only if*

$$\rho(\Phi_A(T,0)) \cdot \rho(\Phi_B(T,0)) < 1.$$

This corollary implies that determining the Floquet multipliers does not require processing the full $4n^2$-dimensional monodromy operator matrix; rather, it suffices to compute the spectral radii of two n-dimensional quaternion matrices in parallel. Assuming the unilateral fundamental solutions Φ_A and Φ_B are acquired, this theorem strictly reduces the eigenvalue computation complexity from $O((4n^2)^3)$ to $2 \times O((4n)^3)$. More importantly, it analytically reveals the independence of left and right dynamics in non-commutatively coupled systems.

3.4. Dissipative Structure and Scalar-Vector Separation Principle of Bilateral Operators

Theorem 4 provides a necessary and sufficient condition for the asymptotic stability of periodic systems from the perspective of spectral radius. However, the linearization analysis of nonlinear Riccati equations requires assessing not only the asymptotic convergence but also the transient growth rate of the solution over finite time intervals. Furthermore, revealing which parts of the coefficient matrices promote growth and which parts merely cause rotation is crucial for understanding physical mechanisms (such as energy conservation in Euler dynamics). To this end, this section introduces operator logarithmic norm theory to reveal the "scalar-vector decoupling" mechanism in bilateral system dynamics.

For any quaternion matrix $X \in M_n(\mathbb{H})$ equipped with the induced spectral 2-norm $\|\cdot\|_2$, the logarithmic norm (or Dahlquist matrix measure) $\mu_2(X)$ is defined via the right directional derivative at zero:

$$\mu_2(X) \triangleq \lim_{h \to 0^+} \frac{\|I_n + hX\|_2 - 1}{h}.$$

Analytically, this limit evaluates the maximum real right eigenvalue of the Hermitian part of X. We define the Hermitian real part as $\mathcal{H}(X) \triangleq \frac{1}{2}(X + X^*)$. Since $\mathcal{H}(X)$ is self-adjoint, its right eigenvalues are strictly real. Consequently, the quaternion logarithmic norm explicitly equates to

$$\mu_2(X) = \lambda_{\max}(\mathcal{H}(X)).$$

This property allows us to bound the continuous evolution of the bilateral system strictly using the algebraically computable Hermitian parts. For two $n \times n$ quaternion matrices X and Y, define their inner product as follows:

$$\langle X, Y \rangle_{\mathbb{H}} = \mathrm{Tr}(X^* Y).$$

Theorem 5. *For the time-varying bilateral linear system (14), the evolution of its solution is strictly controlled by the Hermitian real parts of the coefficient matrices $A(t)$ and $B(t)$, and is independent of their anti-Hermitian imaginary parts. Specifically, for any $t \geq t_0$, the modulus of the solution satisfies the following logarithmic norm estimate:*

$$\|q(t)\| \leq \|q(t_0)\| \exp\left(\int_{t_0}^{t} [\lambda_{\max}(\mathcal{H}(A(\tau))) + \lambda_{\max}(\mathcal{H}(B(\tau)))] d\tau \right). \tag{17}$$

where $\lambda_{\max}(\cdot)$ denotes the maximum real eigenvalue of a self-adjoint quaternion matrix.

Proof. To overcome the non-commutativity of quaternion multiplication and rigorously handle bilateral operators, we examine the induced norm evolution of the fundamental solution matrix $\Phi(t, t_0) \in M_n(\mathbb{H})$ of system (14). Since any solution satisfies $q(t) = \Phi(t, t_0) q(t_0)$, controlling the Frobenius norm of Φ suffices to control the Euclidean norm of the solution:

$$\|q(t)\| = \|\Phi(t, t_0) q(t_0)\| \leq \|\Phi(t, t_0)\|_F \|q(t_0)\|_F. \tag{18}$$

Consider $V(t) = \frac{1}{2}\|\Phi(t)\|_F^2 = \frac{1}{2}\mathrm{Re}[\mathrm{Tr}(\Phi^* \Phi)]$. Differentiating $V(t)$ along the system trajectory:

$$\dot{V}(t) = \mathrm{Re}\langle \dot{\Phi}, \Phi \rangle_{\mathbb{H}} = \underbrace{\mathrm{Re}\langle A\Phi, \Phi \rangle_{\mathbb{H}}}_{T_1} + \underbrace{\mathrm{Re}\langle \Phi B, \Phi \rangle_{\mathbb{H}}}_{T_2}.$$

Upper bounds for T_1 and T_2 are established as follows. Using the linear property of trace and the decomposition of A, we have

$$T_1 = \mathrm{Re}[\mathrm{Tr}(\Phi^* A \Phi)] = \mathrm{Tr}\left(\Phi^* \frac{A + A^*}{2} \Phi\right).$$

Let $\mathcal{H}(A) = \frac{A+A^*}{2}$. Since $\mathcal{H}(A)$ is a self-adjoint matrix, according to the quaternion matrix variational principle, its quadratic form is bounded by the maximum eigenvalue:

$$T_1 \leq \lambda_{\max}(\mathcal{H}(A))\|\Phi\|_F^2.$$

Since the term $T_2 = \mathrm{Re}\langle \Phi B, \Phi \rangle$ involves a right multiplication operator, the cyclicity of the trace operator does not generally hold in the non-commutative quaternion domain. This limitation is circumvented by mapping the problem to the real vector space via the isometric isomorphism $\nu : M_n(\mathbb{H}) \to \mathbb{R}^{4n^2}$.

$$T_2 = \mathrm{Re}\langle \Phi B, \Phi \rangle_{\mathbb{H}} = \langle \nu(\Phi B), \nu(\Phi) \rangle_{\mathbb{R}}.$$

By Lemma 1, we have

$$T_2 = \nu(\Phi)^\top (\mathbf{B}_R^\top \otimes I_{4n}) \nu(\Phi).$$

This is a real quadratic form. Its upper bound is determined by the maximum eigenvalue of the symmetric part of the intermediate real matrix:

$$T_2 \leq \lambda_{\max}\left(\mathrm{Sym}(\mathbf{B}_R^\top \otimes I_{4n})\right) \|\nu(\Phi)\|^2.$$

Consider the structure of this symmetric matrix:

$$\mathrm{Sym}(\mathbf{B}_R^\top \otimes I_{4n}) = \frac{1}{2}\left[(\mathbf{B}_R^\top \otimes I) + (\mathbf{B}_R \otimes I)\right] = \frac{1}{2}(\mathbf{B}_R^\top + \mathbf{B}_R) \otimes I.$$

Since $(\mathbf{B}_R)^\top = (\mathbf{B}^*)_R$, we have

$$\frac{1}{2}(\mathbf{B}_R^\top + \mathbf{B}_R) = \left(\frac{B^* + B}{2}\right)_R = (\mathcal{H}(B))_R.$$

According to quaternion matrix spectral theory, the real eigenvalue spectrum of the right real representation $(\mathcal{H}(B))_R$ of the self-adjoint matrix $\mathcal{H}(B)$ is numerically identical to its own real eigenvalue spectrum (with multiplicity 4). Therefore, it satisfies

$$\lambda_{\max}(\mathrm{Sym}(\mathbf{B}_R^\top \otimes I)) = \lambda_{\max}(\mathcal{H}(B)).$$

Since $\|\nu(\Phi)\|_{\mathbb{R}^{4n^2}} = \|\Phi\|_{F,\mathbb{H}}$, we obtain the precise estimate:

$$T_2 \leq \lambda_{\max}(\mathcal{H}(B))\|\Phi\|_F^2.$$

Substituting the estimates of T_1 and T_2 back into $\dot{V}(t)$:

$$\frac{1}{2}\frac{d}{dt}\|\Phi\|_F^2 \leq [\lambda_{\max}(\mathcal{H}(A(t))) + \lambda_{\max}(\mathcal{H}(B(t)))]\|\Phi\|_F^2.$$

Applying Gronwall's inequality for integration, combined with (18), yields the theorem conclusion (17). □

3.5. Spectral Dichotomy and Riesz Projection of Bilateral Autonomous Systems

In Theorem 5, we established the transient energy growth bound for general time-varying systems using logarithmic norms. However, for the geometric structure of dynamical systems (such as the direct sum decomposition of stable/unstable subspaces),

modulus estimation alone is insufficient. To rigorously analyze the relationship between the spectral structure of bilateral operators and invariant subspaces, and to establish a theoretical foundation for equilibrium point analysis in nonlinear systems, this section examines constant-coefficient bilateral systems under frozen time. Using holomorphic functional calculus, we establish the following more refined dichotomy theorem.

3.5.1. Spectrum and Resolvent of Bilateral Operators

Consider the constant bilateral operator $\mathcal{L}[X] \triangleq AX + XB$ defined on the quaternion matrix space $M_n(\mathbb{H})$. To construct projections, we first need to clarify its spectral structure and resolvent operator. We view $M_n(\mathbb{H})$ as a $4n^2$-dimensional Banach space over the real field.

Definition 5. *Let $\sigma(\mathbf{A}_L), \sigma(\mathbf{B}_R) \subset \mathbb{C}$ be the complex eigenvalue spectra of the left and right real representation matrices of quaternion matrices $A, B \in M_n(\mathbb{H})$, respectively. The operator $\mathcal{L}$ is said to satisfy the non-resonant hyperbolic condition if for any $\lambda \in \sigma(\mathbf{A}_L)$ and $\mu \in \sigma(\mathbf{B}_R)$, we have*

$$Re(\lambda) + Re(\mu) \neq 0. \tag{19}$$

This condition ensures that the spectrum $\sigma(\mathcal{L})$ of operator $\mathcal{L}$ does not intersect the imaginary axis, thereby dividing the complex plane into two disjoint regions: $\mathbb{C}^- = \{z \mid Re(z) < 0\}$ and $\mathbb{C}^+ = \{z \mid Re(z) > 0\}$.

Definition 6. *For a complex number $\xi \in \mathbb{C} \setminus \sigma(\mathcal{L})$, define the bilateral resolvent operator $\mathcal{R}(\xi, \mathcal{L}) \triangleq (\xi\mathcal{I} - \mathcal{L})^{-1}$. For any $Y \in M_n(\mathbb{H})$, the action result $X = \mathcal{R}(\xi, \mathcal{L})[Y]$ is the unique solution to the generalized Sylvester equation [20]:*

$$\xi X - AX - XB = Y. \tag{20}$$

3.5.2. Riesz Projection Theorem

Based on the resolvent operator, we use contour integration to construct projections that decompose the phase space into a stable subspace E^s and an unstable subspace E^u.

Theorem 6. *If constant matrices A, B satisfy condition (19), then the operator $\mathcal{L}$ possesses an exponential dichotomy on $M_n(\mathbb{H})$. The phase space can be decomposed into a direct sum $M_n(\mathbb{H}) = E^s \oplus E^u$, where the spectral projection operator $\mathcal{P}_s$ corresponding to the stable subspace E^s has the following explicit representation based on complex contour integration: for any $X \in M_n(\mathbb{H})$,*

$$\mathcal{P}_s[X] = \frac{1}{2\pi \mathrm{i}} \oint_\Gamma \mathcal{R}(\xi, \mathcal{L})[X] d\xi. \tag{21}$$

where i is the imaginary unit in the complex plane (satisfying $\mathrm{i}^2 = -1$, and commuting with quaternion bases $\mathbf{i}, \mathbf{j}, \mathbf{k}$); $\Gamma \subset \mathbb{C}^-$ is a simple closed Jordan curve enclosing all spectral points of $\mathcal{L}$ in the left half-plane, and Γ is chosen to be symmetric with respect to the real axis; $\mathcal{R}(\xi, \mathcal{L})$ is the resolvent operator in Definition 6.

Proof. Using the vectorization isomorphism ν, according to (10), the spectrum of operator $\mathcal{L}$ is equivalent to the spectrum of its real representation matrix $\mathbf{M}_\mathcal{L} = I \otimes \mathbf{A}_L + \mathbf{B}_R^\top \otimes I$. Since $\sigma(\mathbf{M}_\mathcal{L}) = \{\lambda + \mu \mid \lambda \in \sigma(\mathbf{A}_L), \mu \in \sigma(\mathbf{B}_R)\}$, condition (19) implies $\forall z \in \sigma(\mathbf{M}_\mathcal{L}), \mathrm{Re}(z) \neq 0$. Thus, the spectrum is strictly separated by the imaginary axis into $\sigma_- \cup \sigma_+$.

Since the quaternion matrix space $M_n(\mathbb{H})$ constitutes a real, rather than a complex, Banach algebra, classical holomorphic functional calculus cannot be applied directly to quaternion operators. Instead, the Riesz projection must be rigorously defined through its exact real embedding. Specifically, the bilateral operator $\mathcal{L}$ is mapped to its real representa-

tion $\mathbf{M}_{\mathcal{L}} \in M_{4n^2}(\mathbb{R})$, which is then naturally embedded into the complex Banach algebra $M_{4n^2}(\mathbb{C})$ where the complex contour integration is formally executed.

Since Γ lies strictly within the resolvent set $\rho(\mathbf{M}_{\mathcal{L}})$, for any ξ on Γ, the linear operator $\xi\mathcal{I} - \mathcal{L}$ is formally invertible, i.e., the Sylvester Equation (20) has a unique solution. Fundamentally, the idempotence of the projection ($\mathcal{P}_s^2 = \mathcal{P}_s$) arises directly from the first resolvent identity: $\mathcal{R}(\xi, \mathcal{L}) - \mathcal{R}(\eta, \mathcal{L}) = (\eta - \xi)\mathcal{R}(\xi, \mathcal{L})\mathcal{R}(\eta, \mathcal{L})$. By evaluating the product of two such integrals over Γ and a slightly larger enclosing contour Γ' via the embedded complexified space, we obtain

$$\mathcal{P}_s^2 = \frac{1}{(2\pi\mathrm{i})^2} \oint_{\Gamma} \oint_{\Gamma'} \frac{\mathcal{R}(\xi, \mathcal{L}) - \mathcal{R}(\eta, \mathcal{L})}{\eta - \xi} d\eta d\xi = \frac{1}{2\pi\mathrm{i}} \oint_{\Gamma} \mathcal{R}(\xi, \mathcal{L}) d\xi = \mathcal{P}_s,$$

where the simplification naturally follows from Cauchy's integral formula. Furthermore, since the resolvent $\mathcal{R}(\xi, \mathcal{L})$ trivially commutes with $\mathcal{L}$, the resulting integral $\mathcal{P}_s$ inherently commutes with the system operator ($\mathcal{P}_s\mathcal{L} = \mathcal{L}\mathcal{P}_s$). Consequently, for any state X belonging to the stable subspace E^s (i.e., $\mathcal{P}_s[X] = X$), its mapping satisfies

$$\mathcal{P}_s[\mathcal{L}[X]] = \mathcal{L}[\mathcal{P}_s[X]] = \mathcal{L}[X].$$

This algebraic sequence explicitly guarantees that $\mathcal{L}[X] \in E^s$, thereby rigorously confirming that E^s is an invariant subspace corresponding to the left-half-plane spectrum σ_-. Finally, because the contour Γ is chosen to be conjugate-symmetric with respect to the real axis and the embedded operator $\mathbf{M}_{\mathcal{L}}$ is a real matrix, the resulting integral strictly resides in the real subspace. By the exact isomorphism of the real representation, this real matrix uniquely pulls back to a legitimate quaternion projection operator on $M_n(\mathbb{H})$. Thus, according to the standard theory of Banach algebras [21], the integral (21) rigorously defines the required spectral projection operator.

(1) We need to prove $\mathbf{P} \in M_{4n^2}(\mathbb{R})$, i.e., prove $\overline{\mathbf{P}} = \mathbf{P}$. First, since $\mathbf{M}_{\mathcal{L}}$ is a real matrix, the resolvent satisfies conjugate symmetry:

$$\overline{\mathbf{R}(\xi)} = (\bar{\xi} I - \overline{\mathbf{M}_{\mathcal{L}}})^{-1} = (\bar{\xi} I - \mathbf{M}_{\mathcal{L}})^{-1} = \mathbf{R}(\bar{\xi}).$$

Taking the conjugate of the definition of the projection operator,

$$\overline{\mathbf{P}} = \overline{\frac{1}{2\pi\mathrm{i}} \oint_{\Gamma} \mathbf{R}(\xi) d\xi} = \frac{1}{-2\pi\mathrm{i}} \oint_{\Gamma} \overline{\mathbf{R}(\xi)} \overline{d\xi}.$$

Let $\eta = \bar{\xi}$. Since the contour Γ is symmetric with respect to the real axis, the point set $\{\bar{\xi} \mid \xi \in \Gamma\}$ is still Γ, but the traversal direction is reversed, denoted as $-\Gamma$; thus, we have

$$\oint_{\Gamma} \mathbf{R}(\bar{\xi}) \overline{d\xi} = \oint_{-\Gamma} \mathbf{R}(\eta) d\eta = -\oint_{\Gamma} \mathbf{R}(\eta) d\eta.$$

Substituting these two terms back into the expression for $\overline{\mathbf{P}}$ yields

$$\overline{\mathbf{P}} = \left(-\frac{1}{2\pi\mathrm{i}}\right)\left(-\oint_{\Gamma} \mathbf{R}(\eta) d\eta\right) = \frac{1}{2\pi\mathrm{i}} \oint_{\Gamma} \mathbf{R}(\eta) d\eta = \mathbf{P}.$$

(2) According to the fundamental theorem of quaternion linear algebra, a real matrix $\mathbf{X}$ is a real representation of some quaternion operator if and only if it commutes with three complex structure matrices J_1, J_2, J_3 (i.e., $\mathbf{X}J_k = J_k\mathbf{X}$). Here, $J_1 = I_n \otimes \chi_R(\mathbf{i}), J_2 = I_n \otimes \chi_R(\mathbf{j}), J_3 = I_n \otimes \chi_R(\mathbf{k})$. Since $\mathbf{M}_{\mathcal{L}}$ originates from the quaternion operator $\mathcal{L}$, it satisfies $\mathbf{M}_{\mathcal{L}}J_k = J_k\mathbf{M}_{\mathcal{L}}$. Also, clearly $J_k\mathbf{R}(\xi) = \mathbf{R}(\xi)J_k$, so

$$\mathbf{P}J_k = \left(\frac{1}{2\pi \mathrm{i}} \oint_\Gamma \mathbf{R}(\xi)d\xi\right) J_k = J_k \left(\frac{1}{2\pi \mathrm{i}} \oint_\Gamma \mathbf{R}(\xi)d\xi\right) = J_k \mathbf{P}.$$

Therefore, $\mathcal{P}_s$ is a legitimate projection operator on $M_n(\mathbb{H})$. □

Remark 1. *While the Riesz projection defined in Equation (21) provides a fundamental topological decomposition via complex contour integration, the explicit analytical evaluation of functions of operators—such as the resolvent $\mathcal{R}(\xi, \mathcal{L}) = (\xi\mathcal{I} - \mathcal{L})^{-1}$, which inherently involves negative powers of operators—can sometimes be analyzed through alternative algebraic avenues. In the broader context of operator dynamics and algebraic structure stability, specific generalizations of polynomials have been introduced to circumvent dense integration. For example, Hermite-Bell polynomials have found significant applications in the exact analysis of negative powers of operators [22]. Although the complex embedding method remains the most direct tool for the quaternion spectral dichotomy derived above, integrating such generalized polynomial tools could present a highly promising avenue for future operational calculus on non-commutative algebras.*

3.5.3. Structural Stability and Projection Differentiation of Slowly Varying Systems

Theorem 6 solves the structural decomposition problem of constant coefficient bilateral systems using holomorphic functional calculus and Riesz projection. However, actual physical processes (such as variable mass rigid body attitude dynamics or control systems with parameter drift) are often non-autonomous. This section extends the dichotomy roughness theory of classical Banach space differential equations to the bilateral quaternion operator space, proving that as long as the system parameters $A(t), B(t)$ drift slowly with time, the "instantaneous stable subspace" determined by Theorem 6 can still effectively capture the asymptotic behavior of the system.

Theorem 7. *Consider the smooth time-varying bilateral system defined on the Banach space $M_n(\mathbb{H})$:*

$$\dot{X}(t) = \mathcal{L}(t)[X(t)] \triangleq A(t)X(t) + X(t)B(t).$$

Assume the system satisfies the following conditions:

1. **Uniform Boundedness:** $\sup_{t\in\mathbb{R}}(\|A(t)\| + \|B(t)\|) \leq M < \infty$.
2. **Uniform Non-resonant Hyperbolicity:** *There exists $\beta > 0$ such that for any $t \in \mathbb{R}$, the distance between the spectrum of the frozen time operator $\mathcal{L}(t)$ and the imaginary axis has a uniform lower bound, i.e., $dist(\sigma(\mathcal{L}(t)), i\mathbb{R}) \geq \beta$.*
3. **Slowly Varying Condition:** *The rate of change of the coefficient matrices is uniformly controlled, i.e., $\sup_{t\in\mathbb{R}}(\|\dot{A}(t)\| + \|\dot{B}(t)\|) \leq \varepsilon$.*

Then there exists a critical threshold $\varepsilon_0 > 0$ depending only on M, β, such that when $\varepsilon < \varepsilon_0$, the time-varying system maintains an exponential dichotomy on $M_n(\mathbb{H})$. Specifically, the evolution of the instantaneous Riesz projection operator $P_s(t)$ satisfies the following explicit operator differential equation:

$$\frac{d}{dt}P_s(t) = \frac{1}{2\pi \mathrm{i}} \oint_\Gamma \mathcal{R}(\xi, t) \circ \left[\dot{A}(t)\mathcal{I} + \mathcal{I}\dot{B}(t)\right] \circ \mathcal{R}(\xi, t)\, d\xi, \tag{22}$$

where $\mathcal{R}(\xi, t) = (\xi\mathcal{I} - \mathcal{L}(t))^{-1}$ is the bilateral resolvent operator at time t, and $\mathcal{I}$ is the identity operator.

Proof. First, taking the time derivative of the bilateral resolvent operator $\mathcal{R}(\xi, t)$ yields

$$\frac{d}{dt}(T(t)^{-1}) = -T(t)^{-1}\dot{T}(t)T(t)^{-1}. \tag{23}$$

Let $T(t) = \xi\mathcal{I} - \mathcal{L}(t)$. Note that ξ is the integration variable, so $\dot{T}(t) = -\dot{\mathcal{L}}(t)$. The derivative of the bilateral operator $\dot{\mathcal{L}}(t)$ is defined as a linear map acting on $Y \in M_n(\mathbb{H})$:

$$\dot{\mathcal{L}}(t)[Y] = \frac{d}{dt}(A(t)Y + YB(t)) = \dot{A}(t)Y + Y\dot{B}(t).$$

Substituting into Formula (23), we obtain the resolvent differential formula:

$$\frac{\partial}{\partial t}\mathcal{R}(\xi, t) = \mathcal{R}(\xi, t) \circ \dot{\mathcal{L}}(t) \circ \mathcal{R}(\xi, t). \tag{24}$$

According to Theorem 6, the instantaneous stable subspace projection is $P_s(t) = \frac{1}{2\pi i}\oint_\Gamma \mathcal{R}(\xi, t)d\xi$. Since the uniform spectral gap condition ensures that the integration contour Γ can be chosen as a fixed curve that does not change with time, differentiating directly with respect to t and substituting Equation (24) yields Equation (22). According to standard estimates in operator theory, the norm of the resolvent operator on the contour Γ surrounding the spectrum is strictly controlled by the spectral distance [23]. Specifically, there exists a constant $C_\Gamma \geq 1$ such that the following estimate holds uniformly:

$$\sup_{\xi\in\Gamma} \|\mathcal{R}(\xi, t)\| \leq \frac{C_\Gamma}{\beta}.$$

Combined with the slowly varying condition $\|\dot{\mathcal{L}}(t)\| \leq \|\dot{A}(t)\| + \|\dot{B}(t)\| \leq \varepsilon$, we have

$$\|\dot{P}_s(t)\| \leq \frac{L(\Gamma)}{2\pi}\left(\frac{C_\Gamma}{\beta}\right)^2 \varepsilon \triangleq K\varepsilon.$$

This indicates that the geometric direction change speed $\dot{P}_s(t)$ of the stable subspace is linearly controlled by the parameter drift speed ε. Proving the dichotomy requires constructing a transformation mapping the time-varying projection $P_s(t)$ to a constant projection $P_0 = P_s(0)$. According to Kato's (1950) adiabatic evolution theory [24], there exists a family of invertible transformation operators $U(t)$ satisfying the following evolution equation:

$$\dot{U}(t) = [\dot{P}_s(t), P_s(t)]U(t), \quad U(0) = \mathcal{I}, \tag{25}$$

where $[\dot{P}_s, P_s] \triangleq \dot{P}_s P_s - P_s\dot{P}_s$. This transformation has the property $P_s(t) = U(t)P_0U(t)^{-1}$. Let $Y(t) = U^{-1}(t)X(t)$, and the original system transforms into

$$\dot{Y}(t) = (\mathbf{\Lambda}(t) + \mathbf{\Delta}(t))Y(t). \tag{26}$$

where the main part is $\mathbf{\Lambda}(t) = U^{-1}(t)\mathcal{L}(t)U(t)$, and the perturbation part $\mathbf{\Delta}(t) = -U^{-1}(t)\dot{U}(t)$. Since $P_s(t)$ commutes with $\mathcal{L}(t)$, the transformed operator $\mathbf{\Lambda}(t)$ must commute with the constant projection P_0. This implies that $\mathbf{\Lambda}(t)$ is block diagonalized, i.e., $\mathbf{\Lambda}(t) = \mathrm{diag}(\mathbf{\Lambda}_s(t), \mathbf{\Lambda}_u(t))$. Since both $\mathcal{L}(t)$ and $U(t)$ are slowly varying operators, it is easy to see that $\mathbf{\Lambda}(t)$ itself is also slowly varying and uniformly hyperbolic. Combined with the logarithmic norm estimate of Theorem 5 and Coppel's classical theory on slowly varying systems, it is known that $\mathbf{\Lambda}(t)$ itself possesses an exponential dichotomy. System (26) presents the form of "main part with exponential dichotomy + small perturbation". According to the classical theorems on roughness by Coppel [25] and Daleckii & Krein [26], as long as the perturbation amplitude $\|\mathbf{\Delta}(t)\|$ is sufficiently small (i.e., ε is below a certain threshold ε_0), the perturbed system $Y(t)$ maintains exponential dichotomy. Since the transformation $U(t)$ is uniformly bounded and invertible, the original system $X(t)$ also maintains exponential dichotomy. □

Remark 2. *To ensure the mathematical completeness of Theorem 7, we can provide an explicit sufficient estimate for the critical threshold ε_0 based on the perturbation theory of Green's operators on Banach spaces. According to the foundational spectral theory by Sacker & Sell [27] and Coppel's classical conclusion on dichotomy roughness [25], if the original frozen system has exponential dichotomy constants (K_0, β), then the dichotomy is maintained when the supremum of the perturbation term $\|\Delta(t)\|$ satisfies the following condition:*

$$\sup_{t\in\mathbb{R}} \|\mathbf{\Delta}(t)\| < \frac{\beta}{2K_0}. \tag{27}$$

The perturbation term originates from the Kato transformation operator $\dot{U} = [\dot{P}_s, P_s]U$. Taking its norm, we have

$$\|\mathbf{\Delta}(t)\| = \| - U^{-1}\dot{U}\| \leq \|U^{-1}\|(2\|\dot{P}_s\|\|P_s\|)\|U\| \leq 2\kappa(U)\|P_s\|\|\dot{P}_s(t)\|,$$

where $\kappa(U)$ is the uniform condition number of the transformation operator. Also $\|\dot{P}_s(t)\| \leq C_{geom}\frac{\varepsilon}{\beta^2}$ (where C_{geom} summarizes geometric constants such as contour length), we obtain the explicit upper bound of the perturbation term:

$$\|\mathbf{\Delta}(t)\| \leq 2\kappa(U)\|P_s\|C_{geom}\frac{\varepsilon}{\beta^2}. \tag{28}$$

Substituting (28) into (27) and solving for ε, we obtain the sufficient condition $\varepsilon < \varepsilon_0$, where

$$\varepsilon_0 = \frac{\beta^3}{4K_0\kappa(U)\|P_s\|C_{geom}}. \tag{29}$$

This expression illustrates the essence of the robustness of bilateral systems: the permissible parameter change rate ε_0 has a cubic relationship with the system's spectral gap β ($\varepsilon_0 \propto \beta^3$). This means that as $\beta \to 0$, the system's tolerance to slowly varying perturbations will drop sharply.

Remark 3. *Although the form of Theorem 7 is similar to the general theory in Banach spaces, its specific meaning in quaternion bilateral systems has significant specificity, mainly reflected in the following two points: 1.* ***Non-commutative Splitting of Tangent Space:*** *The perturbation source term $\dot{\mathcal{L}} = \dot{A}\mathcal{I} + \mathcal{R}_{\dot{B}}$ in Formula (22) illustrates the special structure of the tangent space of the system parameter manifold. In commutative algebras, the bilateral system degenerates into a unilateral system, and the rate of change is determined only by a single matrix $\dot{A} + \dot{B}$. In the quaternion domain, due to $\dot{A}q \neq q\dot{A}$, the left perturbation $\dot{A}$ and the right perturbation $\dot{B}$ are linearly independent. Theorem 7 proves that such independent left and right perturbations will not destroy the overall spectral separation structure, as long as their resultant force (i.e., the real part of the spectral sum) maintains hyperbolicity. 2.* ***Complementary Stability Mechanism:*** *Classical unilateral system stability requires $Re(\sigma(A)) \neq 0$. However, the spectral gap condition $|Re(\lambda) + Re(\mu)| \geq \beta$ of bilateral systems allows both $A(t)$ and $B(t)$ to be unstable. For example, if $Re(\sigma(A)) \subset [1, 2]$ (unstable) and $Re(\sigma(B)) \subset [-4, -3]$ (strongly stable), then the spectral sum lies in $[-3, -1]$, and the system as a whole is not only stable but also has robust dichotomy. This mechanism of "compensating" for left-side instability through the right-side operator is a unique advantage in the design of quaternion bilateral control systems and is also where this theorem differs from standard unilateral theory.*

Remark 4. *The cubic robustness law, $\varepsilon_0 \sim \mathcal{O}(\beta^3)$, established in Theorem 7, fundamentally relies on a slowly varying assumption, implicitly requiring the parametric perturbation frequency to be sufficiently decoupled from the system's internal eigenvalues. For fast-varying systems subject to high-frequency excitations, transient dynamics and resonant cross-couplings can strictly dominate*

the bilateral evolution. Under such conditions, the higher-order error terms in the perturbation expansion are no longer negligible, which may degrade the cubic robustness bound to a lower-order scaling or even induce parametric instability. Generalizing this robustness topology to arbitrarily fast-varying environments remains non-trivial and would likely necessitate entirely different operator-theoretic tools, such as high-frequency averaging theories or the continuous Magnus expansion.

4. Quaternion Chebyshev Spectral Collocation Method and Structure Preservation

In the preceding Section 3, we established the operator spectral stability theory for bilateral linear systems, particularly Theorem 5, which revealed the dissipative-rotational decoupling structure of system evolution, and Theorem 7, which established robustness under slowly varying conditions. To accurately replicate these dynamic features numerically and achieve high-precision approximations of the Floquet multipliers, this section embeds the Quaternion Chebyshev Spectral Collocation Method (Q-CSCM) into the aforementioned isomorphic framework to guarantee structural fidelity.

Unlike low-order methods based on local Taylor expansions, spectral methods [28,29] natively achieve exponential convergence for smooth solutions by approximating functions with global orthogonal polynomials. As is well known in classical numerical analysis, this exponential decay is an intrinsic property of the Chebyshev approximation itself, rather than a novel phenomenon generated by the quaternion algebra. Consequently, the core methodological innovation of this section lies in the rigorous, structure-preserving algebraic construction of the fully discrete matrix $\mathcal{M}_{\text{global}}$. Our Kronecker-product-based mapping ensures that the non-commutative bilateral quaternion dynamics can safely and exactly inherit this intrinsic Chebyshev spectral accuracy, without destroying the underlying 4×4 symplectic symmetries or introducing spurious, physically meaningless eigenvalues during the real vectorization process.

4.1. Function Spaces and Orthogonal Approximation

Establishing a rigorous error analysis framework requires extending classical approximation theory to non-commutative quaternion functional spaces.

If the original system is defined on a general interval $t \in [0, T]$, we map it to the standard Chebyshev interval $\tau \in [-1, 1]$ via the affine transformation $\tau = \frac{2t}{T} - 1$. The corresponding differential operator transformation is $\frac{d}{dt} = \frac{2}{T}\frac{d}{d\tau}$. To simplify notation, the following discussion assumes the standard interval $[-1, 1]$, and t is still used to denote the independent variable.

Recall the real vectorization operator $\nu : \mathbb{H}^n \to \mathbb{R}^{4n}$ defined in Section 2.3. To ensure consistency of norms in numerical analysis, we clarify its geometric properties here. According to the quaternion modulus definition $|q|^2 = \sum q_m^2$, the map ν satisfies Euclidean norm isometry:

$$\|\nu(\mathbf{Q})\|_{\mathbb{R}^{4n}} = \|\mathbf{Q}\|_{\mathbb{H}^n}, \quad \forall \mathbf{Q} \in \mathbb{H}^n.$$

Also, it satisfies the consistency of the real part of the inner product, i.e., $\langle \nu(P), \nu(Q) \rangle_{\mathbb{R}} = \text{Re}\langle P, Q \rangle_{\mathbb{H}}$.

Let $\omega(t) = (1 - t^2)^{-1/2}$ be the Chebyshev weight function of the first kind. We define the quaternion-weighted Hilbert space $L^2_\omega([-1, 1]; \mathbb{H}^n)$. Because quaternion multiplication is non-commutative, directly defining the inner product as $\int \bar{u} v$ may yield non-real

values, which violates the axioms of a Hilbert space. This issue is resolved by utilizing the isomorphism ν to rigorously define the L^2 inner product as a real integral:

$$\langle u, v\rangle_{L^2_\omega} \triangleq \int_{-1}^{1} \nu(u(t))^\top \nu(v(t))\omega(t)dt. \tag{30}$$

The corresponding induced norm is $\|u\|_{L^2_\omega} = \sqrt{\langle u, u\rangle_{L^2_\omega}}$. On this basis, define the s-order quaternion weighted Sobolev space $H^s_\omega(\mathbb{H}^n)$ [30]. This space constitutes a Hilbert space, with its Sobolev inner product defined as the accumulation of the L^2 inner products of derivatives of each order:

$$\langle u, v\rangle_{H^s_\omega} \triangleq \sum_{k=0}^{s} \langle u^{(k)}, v^{(k)}\rangle_{L^2_\omega}. \tag{31}$$

The corresponding Sobolev norm induced by the inner product is

$$\|u\|_{H^s_\omega} = \sqrt{\langle u, u\rangle_{H^s_\omega}} = \left(\sum_{k=0}^{s} \|u^{(k)}\|^2_{L^2_\omega}\right)^{1/2}. \tag{32}$$

To discretize the system, we select Gauss–Lobatto collocation points:

$$t_j = \cos\left(\frac{\pi j}{N}\right), \quad j = 0, 1, \ldots, N.$$

This constitutes a non-uniform discrete grid containing $N+1$ nodes. Based on this node set, define the discrete weighted inner product on the fully discrete vector space:

$$\langle \mathbf{u}, \mathbf{v}\rangle_N \triangleq \sum_{j=0}^{N} \varpi_j \nu(u_j)^\top \nu(v_j), \tag{33}$$

where ϖ_j are the Chebyshev–Gauss–Lobatto quadrature weights:

$$\varpi_j = \begin{cases} \frac{\pi}{2N}, & j = 0, N, \\ \frac{\pi}{N}, & 1 \le j \le N-1. \end{cases}$$

The corresponding discrete norm is defined as $\|\mathbf{u}\|_N = \sqrt{\langle \mathbf{u}, \mathbf{u}\rangle_N}$. Furthermore, the discrete norm and the continuous L^2_ω norm satisfy the following uniform equivalence relation (for any polynomial v_N of degree N):

$$\|v_N\|_{L^2_\omega} \le \|\mathbf{v}\|_N \le \sqrt{2}\|v_N\|_{L^2_\omega}. \tag{34}$$

Remark 5. *This discrete inner product is a high-order quadrature approximation of the continuous inner product $\langle\cdot,\cdot\rangle_{L^2_\omega}$. For quaternion polynomial products of degree less than $2N-1$, this discrete inner product is exactly equal to the continuous inner product.*

The discrete vector itself has no derivative definition; its regularity is induced by the interpolation polynomial. Define the discrete Sobolev norm as the continuous Sobolev norm of its corresponding interpolation function:

$$\|\mathbf{v}\|_{H^s_N} \triangleq \|v_N\|_{H^s_\omega}. \tag{35}$$

Let $\mathbb{P}_N(\mathbb{H}^n)$ denote the space of quaternion polynomials of degree not exceeding N. Any numerical solution $q_N \in \mathbb{P}_N(\mathbb{H}^n)$ can be uniquely represented as a series expansion of Chebyshev polynomials $T_k(t)$:

$$q_N(t) = \sum_{k=0}^{N} \hat{c}_k T_k(t), \quad \hat{c}_k \in \mathbb{H}^n.$$

It is worth noting that the specific choice of Chebyshev polynomials $T_k(t)$ in the Q-CSCM framework is primarily dictated by their optimality in polynomial interpolation on the bounded interval $[-1, 1]$, which effectively minimizes the Lebesgue constant and mitigates Runge's phenomenon. From a broader perspective of functional bases in Hilbert spaces, contemporary literature has also extensively explored the deep structural connections among other families of polynomials. For instance, the profound similarities between exponential polynomials and Hermite polynomials have been rigorously investigated [31]. While our current methodology relies on the Chebyshev basis for its superior boundary behavior in finite time domains, acknowledging these broader polynomial relationships is crucial for understanding the complete structure of functional bases and extending such spectral frameworks in future studies.

Remark 6. *The Chebyshev basis functions $T_k(t)$ are real-valued functions. In quaternion algebra, real numbers belong to the center, i.e., they commute with any quaternion: $T_k(t)\hat{c}_k = \hat{c}_k T_k(t)$. This algebraic property is crucial; it ensures that the linear structure of the polynomial space is completely consistent with the commutative algebra case, thus eliminating the need to distinguish between "left basis" or "right basis".*

Lemma 2 (Quaternion Jackson Approximation Theorem)**.** *For any sufficiently smooth function $q \in H^s_\omega(\mathbb{H}^n)$ ($s \geq 1$), its interpolation truncation error satisfies the following estimate:*

$$\|q - \mathcal{I}_N q\|_{L^2_\omega} \leq CN^{-s}\|q\|_{H^s_\omega}, \quad \|(q - \mathcal{I}_N q)'\|_{L^2_\omega} \leq CN^{1-s}\|q\|_{H^s_\omega}, \tag{36}$$

where $\mathcal{I}_N$ is the interpolation operator, and the constant C is independent of N.

Proof. Since the isomorphism ν is linear isometric and the basis functions $T_k(t)$ are real-valued, this conclusion is directly obtained by applying the classical Jackson theorem over the real field (see Canuto et al., 2006, Chapter 5) [30] component-wise. □

4.2. Algebraic Construction and Structure Conservation of Spectral Differentiation Matrices

This section transforms the abstract bilateral operator equation into a fully discrete linear algebraic system. Using tensor product tools, we explicitly derive the discrete matrix structure containing the non-commutative multiplication term $\dot{Q} = AQ + QB$ and prove the closure of this discretization scheme within the real representation algebra.

Consider the non-homogeneous bilateral matrix differential equation defined on $t \in [-1, 1]$:

$$\dot{Q}(t) - A(t)Q(t) - Q(t)B(t) = F(t), \tag{37}$$

where the state variable is $Q(t) \in M_n(\mathbb{H})$.

4.2.1. Tensor Product Structure of Fully Discrete State Space

Select $N + 1$ Chebyshev–Gauss–Lobatto collocation points $\{t_j\}_{j=0}^N$, where $t_j = \cos(\pi j/N)$. Constructing the fully discrete equation requires defining the vector space that contains the discrete solution.

Let $\mathcal{V}_N \cong \mathbb{R}^{N+1}$ denote the discrete node value space on the time grid. This space is isomorphic to the N-th degree real polynomial space $\mathbb{P}_N(\mathbb{R})$ via the Lagrange interpolation

map: for any vector $\mathbf{v} \in \mathcal{V}_N$, there exists a unique interpolation polynomial $p(t)$ such that $p(t_j) = (\mathbf{v})_j$.

Let $\mathcal{V}_{\mathbb{H}} \cong \mathbb{R}^{4n^2}$ be the real isomorphic space of the quaternion matrix space $M_n(\mathbb{H})$ under the map ν. We define the fully discrete state vector $\mathbf{Q}$ as an element of the tensor product of these two spaces, i.e., $\mathbf{Q} \in \mathcal{V}_N \otimes \mathcal{V}_{\mathbb{H}} \cong \mathbb{R}^{4n^2(N+1)}$. Specifically, it is an ordered stack of the real vectorized forms of the states at all time instants:

$$\mathbf{Q} = \begin{pmatrix} \nu(Q(t_0)) \\ \vdots \\ \nu(Q(t_N)) \end{pmatrix}, \tag{38}$$

where $\nu : M_n(\mathbb{H}) \to \mathbb{R}^{4n^2}$ is the real vectorization isometric isomorphism defined in Section 2.3.

4.2.2. Kronecker Product Construction of Discrete Operators

Based on the aforementioned tensor product space structure and the vectorization identity in Lemma 1, we construct the matrix representations of the differential operator and the bilateral algebraic operator on the fully discrete space, respectively.

I. Time Domain Differential Operator: Let $D_N \in M_{N+1}(\mathbb{R})$ be the standard Chebyshev spectral differentiation matrix [32], which maps the node value vector to the derivative value vector. Since the time differentiation operation acts on the $\mathcal{V}_N$ space and is decoupled from the quaternion algebraic structure $\mathcal{V}_{\mathbb{H}}$, the full time domain differentiation matrix $\mathbf{D}_{\text{global}}$ is given by the following Kronecker product:

$$\mathbf{D}_{\text{global}} = D_N \otimes I_{4n^2} \in M_{4n^2(N+1)}(\mathbb{R}), \tag{39}$$

where I_{4n^2} is the identity operator of the algebraic space.

II. Bilateral Algebraic Operator: For a fixed time t_j, the instantaneous operator $\mathcal{L}(t_j)[Q] = A(t_j)Q + Q(t_j)B(t_j)$ acts only on the algebraic space $\mathcal{V}_{\mathbb{H}}$. Its real matrix representation $\mathbf{M}_{\mathcal{L}}(t_j) \in M_{4n^2}(\mathbb{R})$ consists of left multiplication and right multiplication parts:

$$\mathbf{M}_{\mathcal{L}}(t_j) = \underbrace{I_n \otimes \mathbf{A}_L(t_j)}_{\text{Left Action}} + \underbrace{\mathbf{B}_R(t_j)^\top \otimes I_n}_{\text{Right Action}}, \tag{40}$$

where $\mathbf{A}_L(t_j), \mathbf{B}_R(t_j) \in M_{4n}(\mathbb{R})$ are the left and right real adjoint matrices of $A(t_j)$ and $B(t_j)$ respectively (defined in Equations (8) and (9)). For the full time domain vector $\mathbf{Q}$, since the spectral collocation method is pointwise decoupled in algebraic operations (i.e., operations at time t_i do not affect t_j), the fully discrete algebraic matrix $\mathcal{M}_{\text{global}}$ exhibits a block diagonal structure:

$$\mathcal{M}_{\text{global}} = \text{blkdiag}(\mathbf{M}_{\mathcal{L}}(t_0), \mathbf{M}_{\mathcal{L}}(t_1), \ldots, \mathbf{M}_{\mathcal{L}}(t_N)). \tag{41}$$

Combining the above constructions, we utilize the core principle of the spectral collocation method to algebraize the operator equation. Note that in the spectral collocation framework, the derivative value vector of the unknown function $Q(t)$ at each node can be approximated by the product of the differentiation matrix and the state vector $\mathbf{D}_{\text{global}}\mathbf{Q}$. Therefore, replacing the differential term with matrix multiplication and the algebraic term with block diagonal matrix action, the original differential Equation (37) transforms into the following linear algebraic system:

$$\left[\mathbf{D}_{\text{global}} - \mathcal{M}_{\text{global}}\right]\mathbf{Q} = \mathbf{F}, \tag{42}$$

where the right-hand side term $\mathbf{F} \in \mathbb{R}^{4n^2(N+1)}$ is defined as the ordered stack of real vectorizations of the non-homogeneous source term $F(t)$ at all collocation points:

$$\mathbf{F} = \begin{pmatrix} \nu(F(t_0)) \\ \vdots \\ \nu(F(t_N)) \end{pmatrix}. \tag{43}$$

For the initial value problem $Q(-1) = Q_{\text{init}}$, note that under the standard Gauss–Lobatto node definition $t_j = \cos(\pi j/N)$, the index $j = N$ corresponds to the start of physical time $t_N = -1$. We replace the $4n^2$ rows corresponding to t_N in the linear system (42) with the initial state constraint equation:

$$\nu(Q(t_N)) = \nu(Q_{\text{init}}).$$

Remark 7. *It is methodologically essential to explicitly distinguish between the analytical complexity reduction achieved in Section 3 and the computational complexity of the global numerical discretization. While Theorem 4 successfully reduces the analytical complexity of computing Floquet multipliers from $\mathcal{O}(n^6)$ to $2 \times \mathcal{O}(n^3)$ assuming the fundamental matrices are acquired, the practical numerical procedure for solving the global boundary value problem via Q-CSCM (i.e., directly inverting the fully discrete matrix $\mathbf{J}_{sys}$) incurs a massive computational cost scaling as $\mathcal{O}(n^6N^3)$. This dense global inversion inherently imposes a severe spatial scalability bottleneck for high-dimensional systems ($n > 1$). Consequently, the claimed efficiency gains of the Q-CSCM algorithm are strictly restrained to its temporal approximation efficiency. By exploiting exponential spectral decay, the required temporal degrees of freedom (N) are drastically minimized, making the direct-inversion scheme exceptionally powerful primarily for low-dimensional ($n = 1$) but highly stiff or oscillatory systems.*

4.2.3. Spectral Structure Conservation of Discrete Operators

The structural fidelity of the fully discrete system fundamentally originates from the exact isometric real representation of the quaternion algebra. Rather than developing a bespoke symplectic time-stepping scheme, our methodology embeds the highly accurate global Chebyshev collocation strictly within this exact algebraic isomorphism. It is crucial to note that the Chebyshev spectral collocation method is fundamentally a generic numerical approximation tool without intrinsic symplectic properties. Therefore, the structural preservation of the underlying 4×4 symplectic symmetries is exclusively guaranteed by the closure of the exact algebraic mapping. We will now rigorously prove that this massive discrete system constructed via isometric vectorization remains mathematically faithful to the quaternion algebra, thereby naturally precluding the emergence of non-physical "spurious modes".

Theorem 8. *The fully discrete operator matrix $\mathcal{M}_{global}$ strictly belongs to the real representation subalgebra of quaternion bilateral linear operators. Specifically, the construction of this matrix ensures that its eigenvalue spectrum $\sigma(\mathcal{M}_{global})$ strictly follows the spectral symmetry constraints of quaternion operators (i.e., eigenvalues appear in pairs according to conjugacy classes). This implies that the fully discrete system inherits spectral fidelity directly from the algebraic mapping, ensuring that the numerical discretization process does not introduce spurious eigenvalues that destroy the physical stability of the system.*

Proof. Define $\mathfrak{gl}_Q(n) \subset M_{4n^2}(\mathbb{R})$ as the set of real matrices corresponding to all bilateral operators of the form $\mathcal{L}[X] = AX + XB$. According to the theory of F. Zhang [1997] [17], matrices in this set possess a specific 4×4 block symplectic symmetry structure. Since for any time node t_j, the local operator matrix is $\mathbf{M}_{\mathcal{L}}(t_j) = I_n \otimes \mathbf{A}_L(t_j) + \mathbf{B}_R(t_j)^\top \otimes I_n$. $\mathbf{A}_L$ is

composed of left multiplication real representation blocks χ_L, which belongs to a legitimate representation. Recalling the definition of $\chi_R(q)$ in Section 2.1, direct calculation shows that its transpose satisfies the following conjugate-transpose duality law:

$$\chi_R(q)^\top = \chi_R(\bar{q}), \quad \forall q \in \mathbb{H}.$$

Extending this property to the block matrix $\mathbf{B}_R = (\chi_R(b_{ij}))_{n\times n}$, we have

$$(\mathbf{B}_R)^\top = (\chi_R(b_{ji})^\top)_{n\times n} = (\chi_R(\bar{b}_{ji}))_{n\times n} = (\mathbf{B}^*)_R.$$

This indicates that $\mathbf{B}_R^\top$ strictly corresponds to the right multiplication real representation of the quaternion matrix B^*. Since B^* is still a legitimate element in $M_n(\mathbb{H})$, $\mathbf{B}_R^\top \otimes I_n \in \mathfrak{gl}_Q(n)$. According to the definition of the fully discrete matrix $\mathcal{M}_{\text{global}}$, we have

$$\sigma(\mathcal{M}_{\text{global}}) = \bigcup_{j=0}^{N} \sigma(\mathbf{M}_{\mathcal{L}}(t_j)).$$

From step 1, it is known that each local sub-block $\mathbf{M}_{\mathcal{L}}(t_j)$ strictly preserves the algebraic structure of the quaternion operator, so its eigenvalue spectrum is completely determined by the quaternion spectra of $A(t_j)$ and $B(t_j)$. The spectrum of the fully discrete matrix must inherit this symmetry, eliminating spurious instability modes caused by improper discretization schemes. □

4.3. Algebraic Stability and Commutator Analysis of Discrete Systems

Traditional convergence analysis of spectral methods typically relies on energy estimates. However, for bilateral quaternion systems, direct energy methods struggle to precisely characterize the independent dynamic contributions of the left and right operators $A(t), B(t)$. To this end, this section proposes a purely algebraic analysis framework based on discrete gauge transformations.

This section utilizes the fundamental solution operators established in Section 3 to construct a decoupled tensor product gauge transformation. This transformation aims to algebraically eliminate the time-varying coupling term $\mathcal{M}_{\text{global}}$ on the left side of the discrete system, thereby transforming the complex variable coefficient stability problem into a perturbation analysis of the "commutator of spectral differentiation matrix and multiplication operator".

4.3.1. Construction of Discrete Gauge Transformation Matrix

Consider the numerical error vector $\mathbf{E} = v(q - q_N)$. Substituting into the fully discrete Equation (42) yields the following non-homogeneous residual equation:

$$\left[\mathbf{D}_{\text{global}} - \mathcal{M}_{\text{global}}\right]\mathbf{E} = \boldsymbol{\tau}_N, \tag{44}$$

where $\boldsymbol{\tau}_N$ is the interpolation truncation error. Proving the invertibility and stability of the coefficient matrix $\mathbf{K} = \mathbf{D}_{\text{global}} - \mathcal{M}_{\text{global}}$ requires algebraically isolating the algebraic operator $\mathcal{M}_{\text{global}}$. Using the unilateral fundamental solution matrices $\Phi_A(t)$ and $\Phi_B(t)$ defined in Theorem 1, we construct the following transformation.

Definition 7. *Based on the vectorization rules of Lemma 1, define the following two block diagonal matrices, corresponding to the left and right dynamic decoupling transformations respectively:*

$$\begin{aligned}
\boldsymbol{\Psi}_L &= blkdiag\Big(I_n \otimes (\boldsymbol{\Phi}_A^{-1}(t_0))_L, \ldots, I_n \otimes (\boldsymbol{\Phi}_A^{-1}(t_N))_L\Big), \\
\boldsymbol{\Psi}_R &= blkdiag\Big((\boldsymbol{\Phi}_B^{-1}(t_0))_R^\top \otimes I_n, \ldots, (\boldsymbol{\Phi}_B^{-1}(t_N))_R^\top \otimes I_n\Big),
\end{aligned} \tag{45}$$

where $\Phi_A^{-1}(t) = \Phi_A(0,t)$ *exists and is smooth. Let the total transformation matrix be* $\mathbf{\Psi} = \mathbf{\Psi}_L \mathbf{\Psi}_R$. *Introduce the transformed error variable* $\mathbf{Y} = \mathbf{\Psi}\mathbf{E}$.

Remark 8. *Here and in the following text, bold symbols (such as* $\mathbf{E}, \mathbf{Y}$*) refer to fully discrete real vectors (*$\in \mathbb{R}^{4n^2(N+1)}$*) vectorized and stacked via the isomorphism map* v. *At the continuous operator level, this transformation corresponds to* $Y(t) = \Phi_A^{-1}(t)E(t)\Phi_B^{-1}(t)$. *According to the differentiation rule, this transformation simplifies the original operator* $\mathcal{L}[E] = \dot{E} - AE - EB$ *to a pure differential operator* $\dot{Y}$; *however, in the discrete spectral space, since the spectral differentiation matrix* $\mathbf{D}_{global}$ *does not satisfy the exact Leibniz rule, this elimination leaves a non-zero commutator error.*

4.3.2. Spectral Differentiation Commutator Lemma

Lemma 3. *Let* $\mathbf{\Psi}$ *be the discrete gauge transformation matrix defined above. Then the full time domain differentiation matrix* $\mathbf{D}_{global}$ *and the inverse transformation matrix* $\mathbf{\Psi}^{-1}$ *satisfy the following operator identity:*

$$\mathbf{D}_{global}\mathbf{\Psi}^{-1} = \mathbf{\Psi}^{-1}\mathbf{D}_{global} + \mathcal{M}_{global}\mathbf{\Psi}^{-1} + \mathbf{R}_{comm}, \tag{46}$$

where $\mathbf{R}_{comm}$ *is the discrete commutator residual. If the coefficient matrices* $A, B \in H^s_\omega$, *then for any discrete vector representing a smooth function* $v \in H^s_N$ *(i.e., corresponding interpolation polynomial* $v_N \in H^s_\omega$*), this residual satisfies the following spectral accuracy estimate:*

$$\|\mathbf{R}_{comm}\mathbf{v}\|_N \leq CN^{1-s}\|\mathbf{v}\|_{H^s_N}. \tag{47}$$

Proof. Consider the fully discrete matrix product $\mathbf{D}_{\text{global}}\mathbf{\Psi}^{-1}$ acting on an arbitrary discrete vector $\mathbf{v}$. Let $v_N(t)$ be the unique interpolation polynomial corresponding to vector $\mathbf{v}$, and define the auxiliary function $F(t) = \Psi^{-1}(t)v_N(t)$.

In the spectral collocation framework, the action of matrix $\mathbf{D}_{\text{global}}$ is to map the node value vector to the derivative value vector of the interpolation polynomial. Therefore, the j-th block (corresponding to time t_j) of the vector $(\mathbf{D}_{\text{global}}\mathbf{\Psi}^{-1}\mathbf{v})$ is exactly equal to the derivative of the interpolation function $\mathcal{I}_N F$:

$$[\mathbf{D}_{\text{global}}(\mathbf{\Psi}^{-1}\mathbf{v})]_j = \nu\left(\frac{d}{dt}(\mathcal{I}_N F)(t_j)\right).$$

Evaluating the exact derivative of $F(t)$ via the Leibniz rule yields

$$\dot{F}(t) = \frac{d}{dt}(\Psi^{-1}v_N) = \dot{\Psi}^{-1}v_N + \Psi^{-1}\dot{v}_N.$$

Since Ψ^{-1} is an evolution operator, satisfying $\dot{\Psi}^{-1} = \mathcal{L} \circ \Psi^{-1}$ (here, $\mathcal{L}$ is the bilateral algebraic operator), the exact derivative satisfies

$$\dot{F}(t) = \mathcal{L}(F(t)) + \Psi^{-1}(t)\dot{v}_N(t).$$

The discrete vector corresponding to the right side of this equation is exactly the value of $(\mathcal{M}_{\text{global}}\mathbf{\Psi}^{-1} + \mathbf{\Psi}^{-1}\mathbf{D}_{\text{global}})\mathbf{v}$ at t_j. From Equation (46), the j-th block of the residual vector satisfies the following exact pointwise equality:

$$[\mathbf{R}_{\text{comm}}\mathbf{v}]_j = \nu\left(\frac{d}{dt}(\mathcal{I}_N F)(t_j) - \dot{F}(t_j)\right) = \nu\big((\mathcal{I}_N F - F)'(t_j)\big).$$

This indicates that $\mathbf{R}_{\text{comm}}\mathbf{v}$ is precisely the discrete projection of the derivative interpolation error of function F at the collocation points.

To rigorously establish the error bound, we explicitly track the accumulation of estimation constants. First, utilizing the discrete-continuous norm equivalence in Formula (34),

there exists an equivalence constant $C_{\text{eq}} \leq \sqrt{2}$ such that the discrete norm of the error is bounded by its continuous weighted L^2_ω norm:

$$\|\mathbf{R}_{\text{comm}}\mathbf{v}\|_N \leq C_{\text{eq}}\|(\mathcal{I}_N F - F)'\|_{L^2_\omega}.$$

Second, applying Lemma 2 directly to the derivative of the interpolation error, we obtain

$$\|(\mathcal{I}_N F - F)'\|_{L^2_\omega} \leq C_{\text{approx}} N^{1-s}\|F\|_{H^s_\omega},$$

where C_{approx} is precisely the generic constant C introduced in Lemma 2. This constant depends intrinsically on the properties of the Chebyshev basis and the domain, but remains strictly independent of the polynomial degree N.

Furthermore, recall that $F(t) = \Psi^{-1}(t)v_N(t)$. Because the fundamental solution operator $\Psi^{-1}(t)$ is generated by smooth coefficient matrices, it acts as a highly regular multiplier. Utilizing the Banach algebra property of Sobolev spaces (i.e., H^s_ω forms an algebra under pointwise multiplication for $s \geq 1$), there exists a boundedness constant $C_\Psi > 0$, determined solely by the continuous H^s_ω-norm of $\Psi^{-1}(t)$, such that

$$\|F\|_{H^s_\omega} = \|\Psi^{-1}v_N\|_{H^s_\omega} \leq C_\Psi\|v_N\|_{H^s_\omega}.$$

Combining the above inequalities and utilizing the discrete Sobolev norm definition (35) (i.e., $\|\mathbf{v}\|_{H^s_N} = \|v_N\|_{H^s_\omega}$), we arrive at the following continuous chain of inequalities:

$$\begin{aligned}\|\mathbf{R}_{\text{comm}}\mathbf{v}\|_N &\leq C_{\text{eq}}\|(\mathcal{I}_N F - F)'\|_{L^2_\omega} \\ &\leq C_{\text{eq}}C_{\text{approx}}N^{1-s}\|F\|_{H^s_\omega} \\ &\leq C_{\text{eq}}C_{\text{approx}}C_\Psi N^{1-s}\|v_N\|_{H^s_\omega} \\ &= CN^{1-s}\|\mathbf{v}\|_{H^s_N}.\end{aligned}$$

Here, the ultimate constant is aggregated as $C = C_{\text{eq}}C_{\text{approx}}C_\Psi$. Since all its constituent parts (C_{eq}, C_{approx}, and C_Ψ) are strictly independent of the discretization parameter N, the aggregated constant C inherently preserves this N-independence. In summary, the lemma is rigorously proved. □

4.3.3. Stability of Discrete Integral Operators

To solve the transformed equation, we need the boundedness of the Chebyshev integral operator (i.e., the generalized inverse of the differentiation matrix).

Lemma 4. *Let $\mathbf{S}_{global} = \mathbf{D}^{\dagger}_{global}$ be the full time domain spectral integration matrix (generalized inverse excluding the initial condition row). Under the weighted norm $\|\cdot\|_N$, there exists a constant C_{int} such that*

$$\|\mathbf{S}_{global}\|_N \leq C_{int}. \tag{48}$$

4.3.4. Spectral Accuracy Convergence Theorem

Theorem 9. *Assume the bilateral system satisfies the conditions of Theorem 7, and the true solution $Q(t) \in H^s_\omega(\mathbb{H}^n)$ ($s \geq 1$). Then the error $\mathbf{E} = \nu(Q - Q_N)$ of the numerical solution Q_N relative to the projection of the true solution satisfies:*

$$\|\mathbf{E}\|_N \leq C \cdot \kappa(\mathcal{U}) \cdot N^{1-s}\|Q\|_{H^s_\omega}, \tag{49}$$

where $\kappa(\mathcal{U}) = \sup_t \|\mathcal{U}(t,0)\|\|\mathcal{U}^{-1}(t,0)\|$ is the condition number of the continuous evolution operator.

Proof. Substitute $\mathbf{E} = \mathbf{\Psi}^{-1}\mathbf{Y}$ into the original error Equation (44):

$$(\mathbf{D}_{\text{global}} - \mathcal{M}_{\text{global}})\mathbf{\Psi}^{-1}\mathbf{Y} = \boldsymbol{\tau}_N.$$

Using the commutator relation (46), we rewrite the operator on the left side as

$$(\mathbf{D}_{\text{global}} - \mathcal{M}_{\text{global}})\mathbf{\Psi}^{-1} = \mathbf{\Psi}^{-1}\mathbf{D}_{\text{global}} + \mathbf{R}_{\text{comm}}.$$

Here, $\mathcal{M}_{\text{global}}\mathbf{\Psi}^{-1}$ is exactly cancelled out, which is precisely the purpose of introducing $\mathbf{\Psi}$. The original equation transforms into

$$(\mathbf{D}_{\text{global}} + \mathbf{\Psi}\mathbf{R}_{\text{comm}})\mathbf{Y} = \mathbf{\Psi}\boldsymbol{\tau}_N.$$

Let us multiply both sides by the integration matrix (using the boundary condition that $\mathbf{Y}$ is 0 at the initial value):

$$(\mathbf{I} + \mathbf{K}_N)\mathbf{Y} = \mathbf{S}_{\text{global}}\mathbf{\Psi}\boldsymbol{\tau}_N,$$

where $\mathbf{K}_N = \mathbf{S}_{\text{global}}\mathbf{\Psi}\mathbf{R}_{\text{comm}}$. According to the compactness theory of spectral methods, the effective norm of the perturbation operator $\mathbf{K}_N$ in the neighborhood of smooth solutions tends to 0 (Note: Strictly speaking, this property depends on the regularity assumption of the solution, i.e., we focus on the action of the operator on smooth components in the finite-dimensional approximation space $\mathbb{P}_N$). Therefore, there exists N_0 such that when $N > N_0$, the operator $(\mathbf{I} + \mathbf{K}_N)$ is invertible, and its inverse operator norm is uniformly bounded:

$$\|(\mathbf{I} + \mathbf{K}_N)^{-1}\|_N \leq \frac{1}{1 - \|\mathbf{K}_N\|_N} \leq C_{\text{stab}}.$$

Thus the transformed error $\mathbf{Y}$ satisfies:

$$\|\mathbf{Y}\|_N \leq C_{\text{stab}}\|\mathbf{S}_{\text{global}}\|_N\|\mathbf{\Psi}\|_N\|\boldsymbol{\tau}_N\|_N.$$

The truncation error $\boldsymbol{\tau}_N$ can now be precisely estimated. Substituting the true solution $Q(t)$ into (42), $\boldsymbol{\tau}_N$ can be expressed as follows:

$$\boldsymbol{\tau}_N = \mathbf{D}_{\text{global}}\nu(Q) - \mathcal{M}_{\text{global}}\nu(Q) - \nu(F).$$

According to the definition of the spectral differentiation matrix $\mathbf{D}_{\text{global}}\nu(Q) = \nu(\frac{d}{dt}(\mathcal{I}_N Q))$, and the true solution satisfying the equation $\dot{Q} = \mathcal{L}Q + F \Rightarrow \nu(\dot{Q}) = \mathcal{M}_{\text{global}}\nu(Q) + \nu(F)$, we rewrite $\boldsymbol{\tau}_N$ as

$$\boldsymbol{\tau}_N = \nu\left(\frac{d}{dt}(\mathcal{I}_N Q)\right) - \nu(\dot{Q}) = \nu\big((\mathcal{I}_N Q - Q)'\big).$$

This indicates that $\boldsymbol{\tau}_N$ is essentially the approximation error of the derivative of the interpolation polynomial. For $Q \in H^s_\omega$, by Formula (36), its derivative interpolation error satisfies

$$\|(\mathcal{I}_N Q - Q)'\|_{L^2_\omega} \leq C_{\text{approx}} N^{1-s}\|Q\|_{H^s_\omega}.$$

Furthermore, using Formula (34),

$$\|\boldsymbol{\tau}_N\|_N \leq C_{\text{cons}} N^{1-s}\|Q\|_{H^s_\omega}.$$

https://doi.org/10.3390/sym18040578

Finally, we revert to the original error variable $\mathbf{E} = \mathbf{\Psi}^{-1}\mathbf{Y}$.

$$\begin{aligned}\|\mathbf{E}\|_N &\leq \|\mathbf{\Psi}^{-1}\|_N \|\mathbf{Y}\|_N \\ &\leq \|\mathbf{\Psi}^{-1}\|_N \cdot \left(C_{\text{stab}} \|\mathbf{S}_{\text{global}}\|_N \|\mathbf{\Psi}\|_N\right) \|\boldsymbol{\tau}_N\|_N \\ &= C_{\text{stab}} \|\mathbf{S}_{\text{global}}\|_N \|\mathbf{\Psi}^{-1}\|_N \|\mathbf{\Psi}\|_N \|\boldsymbol{\tau}_N\|_N \\ &= C_{\text{stab}} \|\mathbf{S}_{\text{global}}\|_N \kappa(\mathbf{\Psi}) \|\boldsymbol{\tau}_N\|_N.\end{aligned}$$

Note that the transformation matrix $\mathbf{\Psi}$ is constructed from discrete sampling of the continuous evolution operator $\mathcal{U}(t, 0)$, so its condition number $\kappa(\mathbf{\Psi})$ asymptotically converges to the condition number $\kappa(\mathcal{U})$ of the continuous operator. Substituting the estimate of $\boldsymbol{\tau}_N$, we obtain the final convergence conclusion:

$$\|\mathbf{E}\|_N \leq (C_{\text{stab}} C_{\text{int}} C_{\text{cons}}) \cdot \kappa(\mathcal{U}) \cdot N^{1-s} \|Q\|_{H^s_\omega}.$$

In summary, the theorem is proven. □

Remark 9. *While Theorem 9 rigorously establishes the theoretical spectral convergence rate, the practical implementation of Q-CSCM must account for the conditioning of the global Kronecker product matrix $\mathbf{J}_{sys}$. In Chebyshev spectral collocation methods for first-order differential equations, the condition number of the differentiation matrix D_N typically scales as $\mathcal{O}(N^2)$, which can amplify floating-point round-off errors for extremely large N. However, the primary practical advantage of Q-CSCM is its exponential convergence, enabling it to reach the machine precision floor with a relatively small number of collocation nodes (e.g., $N \leq 64$). Within this low-N regime, the condition number of the tensor-structured Jacobian remains entirely manageable for standard double-precision arithmetic, as will be verified in subsequent numerical simulations. For exceptionally long-time integration or highly stiff systems where a larger temporal resolution is inevitable, this structural sensitivity is classically resolved in the literature [32,33] by adopting a spectral integration formulation, employing preconditioned Krylov subspace solvers, or utilizing multi-domain spectral element techniques.*

5. Numerical Experiments and Verification

To validate the theoretical criteria (Section 3) and evaluate the proposed numerical framework (Section 4), this section presents a series of numerical experiments conducted in MATLAB 2023b. The proposed Q-CSCM is benchmarked against three baselines: the explicit fourth-order Runge–Kutta (ERK4), the structure-preserving Gauss-Legendre implicit Runge–Kutta (GL-IRK4), and the Legendre Spectral Collocation Method (Q-LSCM).

Scope of Applicability and Numerical Challenges: As discussed in Section 4.2.2, the algorithm's reliance on dense global matrix inversion currently limits its spatial scalability. Consequently, this numerical validation is strictly confined to scalar quaternion systems ($n = 1$, corresponding to 4D real dynamical systems). To rigorously assess the methodology within this defined scope, the experiments target severe dynamic conditions that typically challenge conventional solvers. Specifically, the test cases encompass: near-critical stability regimes with Hopf bifurcations (Section 5.2.1), systems exhibiting strong high-frequency rotational stiffness (Section 5.2.2), and extended-horizon nonlinear boundary value problems for heteroclinic connections (Section 5.3.4).

The implementation relies on two core routines. Algorithm 1 employs a Newton–Raphson scheme with explicit Kronecker-product Jacobian construction to ensure structure-preserving spectral accuracy. Algorithm 2 extends this framework to heteroclinic problems, utilizing a homotopy-based continuation strategy to overcome error accumulation in extended-horizon integrations.

5.1. Convergence Analysis and Computational Efficiency

To verify the spectral accuracy characteristics of the algorithm, we selected a specific non-homogeneous time-varying bilateral quaternion differential equation as a benchmark test case. The design of this case aims to cover strong coupling effects between scalar and vector parts as well as multi-frequency oscillation characteristics.

Algorithm 1 Q-CSCM with Newton-Raphson Iteration for Nonlinear Bilateral QDEs

Input: System functions $f(t,q)$ (e.g., $qa(t)q + c(t)$) and its Fréchet derivative; Time period T; Collocation number N; Tolerance ϵ; Max iterations K_{max}.
Output: Discrete solution vector $\mathbf{Q} \in \mathbb{R}^{4n(N+1)}$.

Step 1: Discretization Setup
Generate Chebyshev-Gauss-Lobatto nodes: $\tau_j = \cos(\pi j/N),\ j = 0, \ldots, N$.
Map to physical time: $t_j = (\tau_j + 1)T/2$.
Construct standard differentiation matrix $D_N \in \mathbb{R}^{(N+1)\times(N+1)}$.
Form global operator with time scaling: $\mathbf{D}_{\text{global}} = (\frac{2}{T} D_N) \otimes I_{4n}$.
Step 2: Initialization
Generate initial guess $\mathbf{Q}^{(0)}$ (e.g., via low-order ODE solver).
Set iteration counter $k = 0$, error $\delta = \infty$.
while $\delta > \epsilon$ **and** $k < K_{max}$ **do**
    Step 3: Assembly of Jacobian and Residual
    Initialize algebraic Jacobian block $\mathbf{J}_{\text{alg}} = \mathbf{0}$ and Residual $\mathbf{R} = \mathbf{0}$.
    for $j = 0$ to N **do**
        Extract local state $q_j = \nu^{-1}(\mathbf{Q}_{[j]}^{(k)})$ and parameters $a_j = a(t_j)$.
        Evaluate vector field: $v_j = q_j a_j q_j + c(t_j)$.
        Compute Fréchet derivative terms: $L_{\text{term}} = q_j a_j,\ R_{\text{term}} = a_j q_j$.
        Construct local Jacobian block $\mathbf{M}_j \in \mathbb{R}^{4n\times 4n}$ using real representations:
            $\mathbf{M}_j = \mathbf{A}_L(L_{\text{term}}) + \mathbf{B}_R(R_{\text{term}})$.
        Assemble: $\mathbf{J}_{\text{alg}} \leftarrow \text{blkdiag}(\mathbf{J}_{\text{alg}}, \mathbf{M}_j)$.
        Compute local residual: $\mathbf{r}_j = \nu(v_j)$.
    end for
    Global Linear System: $\mathbf{J}_{\text{sys}} = \mathbf{D}_{\text{global}} - \mathbf{J}_{\text{alg}}$; $\mathbf{R}_{\text{sys}} = \mathbf{D}_{\text{global}}\mathbf{Q}^{(k)} - \mathbf{r}_{\text{vec}}$.
    Step 4: Boundary Conditions (Periodic)
    Replace the last block row of $\mathbf{J}_{\text{sys}}$ and $\mathbf{R}_{\text{sys}}$:
    $\mathbf{J}_{\text{sys}}(\text{end}, :) \leftarrow [\mathbf{I}_{4n}, \mathbf{0}, \ldots, \mathbf{0}, -\mathbf{I}_{4n}]$; $\mathbf{R}_{\text{sys}}(\text{end}) \leftarrow \mathbf{Q}_0^{(k)} - \mathbf{Q}_N^{(k)}$.
    Step 5: Update
    Solve linear system: $\mathbf{J}_{\text{sys}}\Delta\mathbf{Q} = -\mathbf{R}_{\text{sys}}$.
    Update with damping $\lambda \in (0, 1]$: $\mathbf{Q}^{(k+1)} = \mathbf{Q}^{(k)} + \lambda\Delta\mathbf{Q}$.
    Update error: $\delta = \|\Delta\mathbf{Q}\|_\infty$.
    $k \leftarrow k + 1$.
end while
return $\mathbf{Q}^{(k)}$.

5.1.1. Problem Setup

Consider the bilateral system defined on the standard interval $t \in [-1, 1]$:

$$\dot{q}(t) = A(t)q(t) + q(t)B(t) + f(t), \quad q(-1) = q_0, \tag{50}$$

where the time-varying coefficient quaternions $A(t)$ and $B(t)$ are defined as

$$A(t) = -0.5 + \cos(t)\mathbf{i} + \sin(t)\mathbf{j}, \quad B(t) = -0.2 + \cos(2t)\mathbf{j} + \sin(2t)\mathbf{k}.$$

To precisely quantify the error, we preset the exact solution of the system as

$$q(t) = e^{\sin(\pi t)} + \cos(t)\mathbf{i} + \cos(5t)\mathbf{j} + \frac{1}{1+t^2}\mathbf{k}.$$

The non-homogeneous source term $f(t)$ is determined by substituting the above exact solution into Equation (50) and calculating backwards. This solution contains exponential functions, trigonometric functions, and rational functions, possessing different smoothness characteristics and frequency components, making it suitable for a comprehensive evaluation of algorithm performance.

Algorithm 2 Robust Continuation for Heteroclinic Connections via Q-CSCM

Input: Source orbit $\mathbf{Q}_{\text{src}}$ and Sink orbit $\mathbf{Q}_{\text{snk}}$ (pre-computed); Initial time horizon T_{init}; Target horizon T_{final}; Step size ΔT.
Output: Heteroclinic trajectory $\mathbf{Q}_{\text{het}}$.
Step 1: Initialization
Set current horizon $T = T_{\text{init}}$.
Initialize solution container $\mathbf{Q}_{\text{sol}} = \emptyset$.
Step 2: Continuation Loop
while $T \leq T_{\text{final}}$ **do**
    2.1: Grid Generation & Initial Guess
    Update collocation nodes $t_j \in [0, T]$ and operator $\mathbf{D}_{\text{global}}$.
    if $T == T_{\text{init}}$ **then**
        Construct $\mathbf{Q}^{(0)}$ using Sigmoid blending (Homotopy):
            $w(t) = [1 + \exp(-2(t - T/2))]^{-1}$.
            $q_{\text{guess}}(t) = (1 - w(t))q_{\text{src}}(t) + w(t)q_{\text{snk}}(t)$.
    else
        Interpolate previous solution $\mathbf{Q}_{\text{prev}}$ to current grid as $\mathbf{Q}^{(0)}$.
    end if
    2.2: Boundary Conditions Setup
    Set Dirichlet BCs anchored to periodic orbits:
        $q_{\text{start}} = q_{\text{src}}(0)$; $q_{\text{end}} = q_{\text{snk}}(T \bmod T_{\text{per}})$.
    2.3: Newton-Raphson Solver (BVP Mode)
    Solve algebraic system $\mathbf{F}(\mathbf{Q}) = \mathbf{0}$ with Jacobian $\mathbf{J}$:
        $\mathbf{J} = \mathbf{D}_{\text{global}} - \mathbf{J}_{\text{alg}}$.
        Apply BCs: Replace first/last block rows of $\mathbf{J}$ and $\mathbf{F}$:
        $\mathbf{J}(1:4,:) \leftarrow [\mathbf{I}, \mathbf{0}, \dots]$; $\mathbf{F}(1:4) \leftarrow q_0 - q_{\text{start}}$.
        $\mathbf{J}(\text{end}-3:\text{end},:) \leftarrow [\dots, \mathbf{0}, \mathbf{I}]$; $\mathbf{F}(\text{end}-3:\text{end}) \leftarrow q_N - q_{\text{end}}$.
    if Solver Converged **then**
        Update $\mathbf{Q}_{\text{prev}} \leftarrow \mathbf{Q}_{\text{sol}}$.
        Increase horizon: $T \leftarrow T + \Delta T$.
    else
        Reduce ΔT and retry.
    end if
end while
return $\mathbf{Q}_{\text{het}} = \mathbf{Q}_{\text{prev}}$.

5.1.2. Comparison of Algebraic Convergence and Spectral Convergence

To rigorously assess the performance of the proposed method and address the inherent asymmetry of comparing a global spectral method solely with local explicit schemes, we compare Q-CSCM against three baselines: the foundational explicit fourth-order Runge–Kutta (ERK4), a state-of-the-art structure-preserving 4th-order Gauss–Legendre Implicit Runge–Kutta (GL-IRK4), and an alternative global approximation scheme, the Quaternion Legendre Spectral Collocation Method (Q-LSCM).

Figure 1a shows the trend of L^∞ error decay as the degrees of freedom (truncation order N for spectral methods, time steps for RK methods) increase. Both the explicit RK4 (orange dashed line) and the implicit symplectic GL-IRK4 (green dash-dotted line) strictly obey the $\mathcal{O}(N^{-4})$ algebraic polynomial decay limit. In stark contrast, both spectral methods (Q-CSCM in blue and Q-LSCM in purple) exhibit strict exponential convergence. Notably, while both spectral bases successfully map to the bilateral quaternion algebra, Q-CSCM

yields a consistently smaller error constant than Q-LSCM. This empirically justifies the choice of Chebyshev nodes, which theoretically possess a superior Lebesgue constant for mitigating Runge-type oscillations near the domain boundaries.

Table 1 quantitatively confirms the algebraic convergence property of the RK methods. As the step size decreases, the experimental order of convergence (EOC) for GL-IRK4 stabilizes at exactly 4.00, dropping only slightly to 3.83 at 5000 steps as the error reaches the machine precision floor (1.1990×10^{-14}). However, reaching this level of precision requires an extremely dense grid of 5000 steps.

Table 2 demonstrates the spectral accuracy advantage of the proposed Q-CSCM over Q-LSCM. With only $N = 32$ collocation points, the L^∞ error of Q-CSCM drops to 8.8899×10^{-10}, which is consistently smaller than the Legendre baseline (1.8491×10^{-9}) at the exact same degrees of freedom. This validates that Q-CSCM achieves superior error constants while maintaining an almost identical, highly efficient computational cost (around 0.0010 s). This result strongly validates Theorem 9.

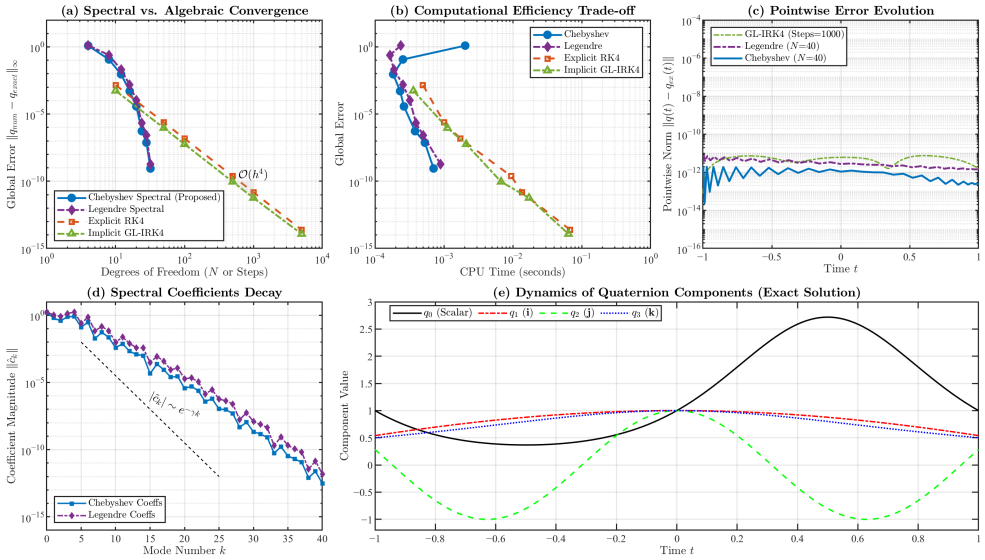


Figure 1. Multi-dimensional performance evaluation of Q-CSCM against the Legendre spectral (Q-LSCM), explicit RK4, and implicit symplectic GL-IRK4 baselines. (**a**) Spectral vs. Algebraic Convergence, highlighting the exponential decay of both Q-CSCM and Q-LSCM versus the $O(h^4)$ decay of the RK methods. Note the slightly superior error constant of the Chebyshev basis. (**b**) Computational efficiency trade-off. (**c**) Pointwise error evolution over time. (**d**) Exponential decay of spectral coefficients for both Chebyshev and Legendre bases. (**e**) Dynamic trajectories of the quaternion components.

5.1.3. Computational Efficiency, Pointwise Error, and Dynamics

Figure 1b illustrates the trade-off between computational cost (CPU time) and solution accuracy. Q-CSCM demonstrates superior performance, achieving optimal accuracy with minimal computational cost. To achieve the same 10^{-10} level of accuracy, Q-CSCM requires significantly less computation time than both the explicit and implicit RK4 methods.

Figure 1c shows the pointwise error distribution over the time domain $[-1, 1]$. While both ERK4 and GL-IRK4 (with $M = 1000$ steps) exhibit noticeable error accumulation reaching the 10^{-11} level, the error of Q-CSCM (with only $N = 40$ points) remains uniformly bounded near machine precision.

5.1.4. Spectral Coefficient Decay and Dynamic Behavior

To further verify the spectral properties, Figure 1d plots the decay of the Chebyshev coefficients $|\hat{c}_k|$, confirming the theoretical exponential decay law $|\hat{c}_k| \sim e^{-\gamma k}$. This

quantitatively confirms that the proposed Q-CSCM framework successfully preserves the intrinsic exponential convergence of the Chebyshev interpolant within the hypercomplex algebraic setting. Finally, Figure 1e presents the time evolution trajectories of the quaternion solution $q(t)$, verifying that Q-CSCM accurately captures complex multi-frequency oscillation behaviors.

Table 1. Grid refinement analysis and algebraic convergence order (EOC) verification for explicit RK4 and implicit symplectic GL-IRK4 baselines.

Steps	ERK4 Error	GL-IRK4 Error	GL-IRK4 Time(s)	GL-IRK4 EOC
10	1.4469×10^{-3}	5.4279×10^{-4}	0.0002	-
50	2.3944×10^{-6}	9.1766×10^{-7}	0.0007	3.97
100	1.5023×10^{-7}	5.7248×10^{-8}	0.0012	4.00
500	2.4070×10^{-10}	9.1657×10^{-11}	0.0065	4.00
1000	1.5047×10^{-11}	5.7285×10^{-12}	0.0150	4.00
5000	2.4314×10^{-14}	1.1990×10^{-14}	0.0572	3.83

Table 2. Spectral accuracy verification and computational efficiency comparison between Legendre (Q-LSCM) and Chebyshev (Q-CSCM) spectral collocation methods.

N	Q-LSCM Error (Legendre)	Q-CSCM Error (Chebyshev)	LSCM Time(s)	CSCM Time(s)
4	1.2953×10^{0}	1.2380×10^{0}	0.0003	0.0008
8	2.4440×10^{-1}	1.1612×10^{-1}	0.0002	0.0003
12	2.0040×10^{-2}	9.1276×10^{-3}	0.0002	0.0002
16	1.4978×10^{-3}	5.1089×10^{-4}	0.0002	0.0002
20	1.0816×10^{-4}	3.6954×10^{-5}	0.0003	0.0003
24	2.0933×10^{-6}	5.3753×10^{-7}	0.0004	0.0005
28	2.6433×10^{-7}	7.4620×10^{-8}	0.0007	0.0004
32	1.8491×10^{-9}	8.8899×10^{-10}	0.0011	0.0010

5.2. Spectral Stability Analysis and Scalar-Vector Separation Verification

This section aims to verify the effectiveness of two core theoretical results from Section 3 through numerical experiments: the precise calculation of bilateral Floquet multipliers based on Theorem 6, and the scalar-vector separation principle based on Theorem 5. We will demonstrate the unique advantages of Q-CSCM in capturing critical dynamic behaviors and preserving geometric structures.

5.2.1. Parametric Floquet Stability and Bifurcation Analysis

For periodic bilateral systems, their long-term stability is determined by the spectral radius $\rho(\mathcal{M})$ of the monodromy operator $\mathcal{M}$. To verify the accuracy and robustness of Q-CSCM in near-critical stability regimes—where numerical diffusion or artificial dissipation can easily lead to false stability conclusions—we consider the following periodic system dependent on a gain parameter μ:

$$\dot{Q} = A(\mu, t)Q + QB(\mu, t), \quad t \in [0, 2\pi],$$

where the coefficient matrices are defined as $A(t) = \mu \sin(t)\mathbf{i} + 0.5\mathbf{k}$ and $B(t) = \cos(t)\mathbf{j} + (\mu - 0.6)\mathbf{1}$. According to Theorem 4, the asymptotic stability of the system is completely determined by the eigenvalue distribution of $\mathcal{M}$. Figure 2 shows the evolution of system stability as parameter μ increases from 0.4 to 0.85.

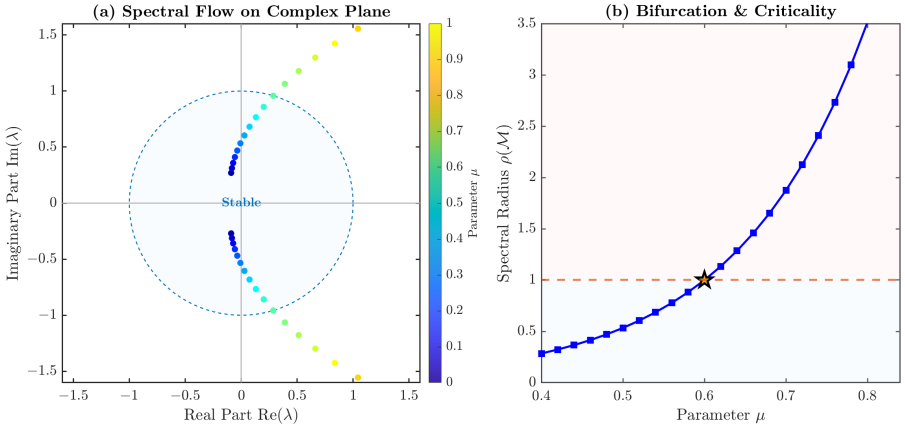


Figure 2. Numerical analysis of Floquet stability and bifurcation behavior. (**a**) Spectral flow on the complex plane: evolution trajectories of Floquet multipliers (monodromy operator eigenvalues) as parameter μ increases. The unit circle (dashed line) marks the stability boundary. Eigenvalues transitioning from blue dots (inside circle) to red dots (outside circle) indicate system instability. (**b**) Bifurcation and criticality: curve of spectral radius $\rho(\mathcal{M})$ versus parameter μ. The intersection with $\rho = 1$ determines the critical bifurcation point μ_c (marked by the pentagram), verifying the dichotomy criterion in Theorem 6.

Figure 2a shows the trajectories of Floquet multipliers (eigenvalues of operator $\mathcal{M}$) in the complex plane. The dashed unit circle ($|\lambda| = 1$) constitutes the stability boundary for discrete maps. As μ increases (color changes from blue to red), eigenvalues migrate from inside the unit circle (stable region) outward and cross the boundary. This spectral crossing precisely characterizes a Hopf-type bifurcation, wherein the system loses stability as the non-resonant hyperbolic condition is violated (Theorem 6).

Figure 2b quantitatively describes the stability margin. The intersection of the spectral radius curve with the critical line $\rho = 1$ precisely locks the bifurcation threshold $\mu_c \approx 0.6$. The curve calculated by Q-CSCM maintains high smoothness and precision near the critical point, avoiding the numerical oscillations frequently observed in low-order algorithms, which confirms the robustness of the method for critical dynamics analysis.

5.2.2. Numerical Verification of Scalar-Vector Separation Principle

Theorem 5 states that the energy evolution of a bilateral system is controlled solely by the Hermitian real parts (dissipative terms) of the coefficient matrices and is strictly decoupled from the anti-Hermitian imaginary parts (rotation terms). To verify this conclusion, we simulated a "stiff" system with time-varying dissipation and strong chaotic rotation:

$$A(t) = \alpha(t) + 100\sin(t^2)\mathbf{i}, \quad B(t) = \beta(t) + 50\cos(t)\mathbf{j}.$$

Figure 3 shows the evolution of the energy norm of the system solution over time. Main plot: The blue solid line (numerical solution) perfectly overlaps with the red dashed line (theoretical upper bound). The theoretical upper bound is given by the formula $\exp(\int(\alpha(t) + \beta(t))d\tau)$. This high consistency confirms that because the exact isometric real representation rigorously preserves the algebraic symmetries of the bilateral operators, the resulting Q-CSCM algorithm naturally avoids introducing spurious artificial dissipation or causing energy divergence, even in the presence of extremely strong rotation term interference. Inset: The green curve shows the local trajectory of a vector component $q_1(t)$. This component exhibits intense high-frequency oscillation driven by the strong imaginary part.

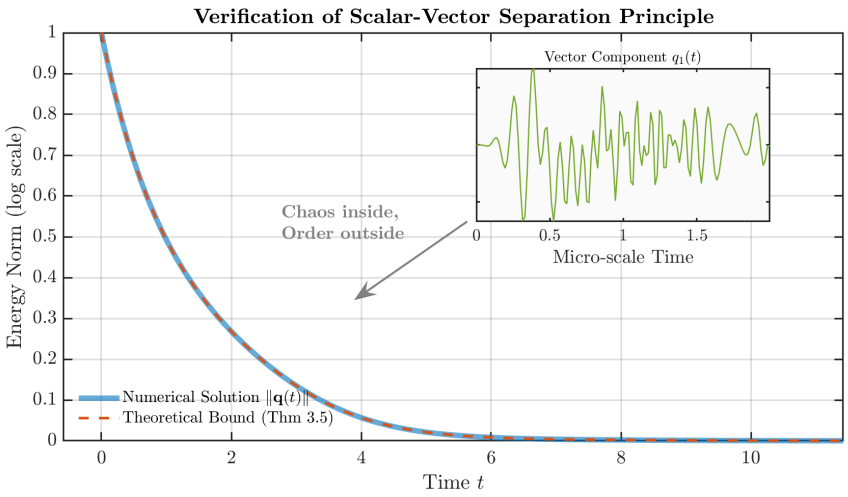


Figure 3. Numerical verification of Scalar-Vector Separation Principle (Theorem 5). Main plot: Comparison of the energy modulus $\|q(t)\|$ of the numerical solution (blue solid line) with the theoretical upper bound calculated based on the Hermitian real parts of the coefficient matrices (red dashed line). The overlapping curves in logarithmic scale confirm that energy decay strictly follows the time-varying dissipation rate. Inset: Time history of vector component $q_1(t)$, showing high-frequency oscillations induced by the anti-Hermitian part.

5.3. Dynamics Analysis and Algorithm Verification of Nonlinear Riccati Oscillator

To further evaluate the performance of Q-CSCM against strongly nonlinear dynamics and extended-horizon boundary value problems, and to verify the applicability of the spectral stability theory proposed in Section 3, this section selects a quaternion Riccati oscillator model with "twisting" characteristics for testing. Based on Wilczyński's theoretical foundation on the existence of periodic solutions, this paper first utilizes Q-CSCM combined with Newton's method to achieve numerical capture of the geometric trajectories of periodic solutions. Subsequently, by constructing the variational equation of this highly nonlinear equation, its stability problem is transformed into a spectral analysis problem of a time-varying bilateral linear system, thereby completing the quantitative determination of the stability of periodic solutions using bilateral Floquet theory.

5.3.1. Problem Setup and Topological Structure of Periodic Orbits

Consider the non-autonomous quaternion Riccati differential equation of the following form [4]:

$$\dot{q}(t) = q(t)A(t)q(t) + C(t), \quad t \in [0, 2\pi],$$

where the coefficient functions $A(t), C(t) \in \mathbb{H}$ contain multi-frequency trigonometric excitation terms, defined as follows:

$$A(t) = -0.5 + \cos(t)\mathbf{i} + 0.3\sin(t)\mathbf{j}, \quad C(t) = -0.1 + 0.2\cos(2t)\mathbf{k}.$$

By selecting different initial guesses, the algorithm successfully converged to two distinct periodic orbits, denoted as Orbit 1 and Orbit 2, respectively.

Figure 4 shows the phase portraits of these two periodic orbits in the three-dimensional imaginary subspace (q_1, q_2, q_3). The blue solid line (Orbit 1) presents a relatively smooth closed curve structure; the orange solid line (Orbit 2) exhibits greater twisting and spatial extension. The projection at the bottom of the figure further reveals significant differences in their geometric topology.

To verify the self-consistency of the numerical solutions, we calculated the internal residuals after Newton iteration convergence. As shown in Table 3, the residuals for both

orbits are below 10^{-13}, indicating that Q-CSCM obtained numerical solutions with machine precision using very few collocation points ($N = 40$).

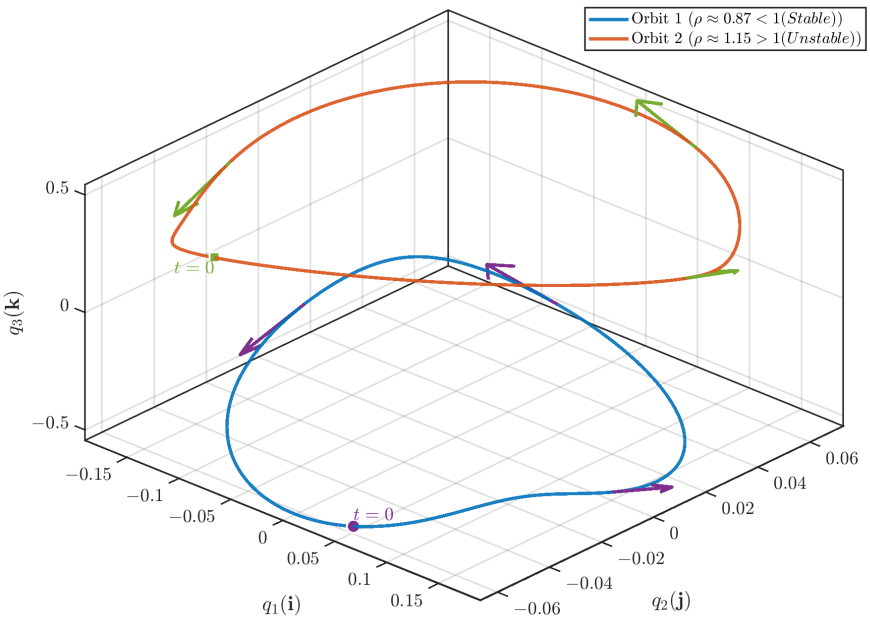


Figure 4. Topological structure of periodic orbits. Trajectories of two coexisting periodic solutions in 3D phase space. The blue curve is the stable orbit (Orbit 1), and the orange curve is the unstable orbit (Orbit 2). The arrows on the curves indicate the direction of temporal evolution along the trajectories. The bottom projection shows the difference in their spatial forms.

Table 3. Numerical residuals and stability statistics of periodic solutions.

Orbit	Stability	Internal Res
Orbit 1	STABLE	5.6399×10^{-14}
Orbit 2	UNSTABLE	5.1070×10^{-15}

5.3.2. Spectral Stability Characteristics and Time Domain Verification

Based on the theory in Section 3, the local stability of a periodic solution of a nonlinear system is determined by the spectral radius $\rho(\mathcal{M})$ of the bilateral monodromy operator of its linearized variational equation.

Figure 5 plots the distribution of Floquet multipliers (eigenvalues) corresponding to Orbit 1 and Orbit 2 in the complex plane. The horizontal and vertical axes represent the real and imaginary parts of the eigenvalues, respectively. The dashed circle represents the unit circle $|\lambda| = 1$, which is the critical boundary for the stability of discrete maps. Blue dots represent multipliers of Orbit 1; all eigenvalues are strictly located inside the unit circle, with spectral radius $\rho_1 \approx 0.8700 < 1$, theoretically determining this orbit as asymptotically stable. Red squares represent multipliers of Orbit 2; there exist eigenvalues distributed outside the unit circle, with spectral radius $\rho_2 \approx 1.1495 > 1$, determining this orbit as unstable.

To verify the physical reality of the above spectral analysis conclusions, we conducted perturbation evolution experiments in the time domain, with results shown in Figure 6. Figure 6a shows that when random initial perturbations are applied to Orbit 1 (black thick line), all perturbation trajectories (blue thin lines) rapidly converge and collapse onto the reference orbit over time, confirming its attractiveness as a limit cycle. Figure 6b shows that after applying small perturbations to Orbit 2, the trajectories (orange thin lines) rapidly diverge and move away from the reference orbit, exhibiting strong repulsion. This time-

domain behavior is completely consistent with the spectral analysis results in Figure 5, verifying the correctness of the bilateral operator spectral theory proposed in this paper for linearization analysis of nonlinear systems.

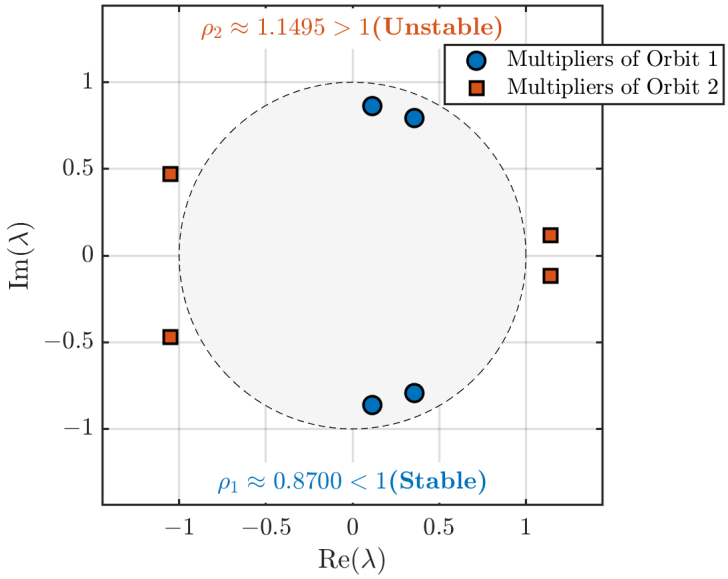


Figure 5. Bilateral Floquet spectral distribution. Eigenvalue distribution of the monodromy operator on the complex plane. Blue dots correspond to Orbit 1, located inside the unit circle (stable); red squares correspond to Orbit 2, partially located outside the unit circle (unstable).

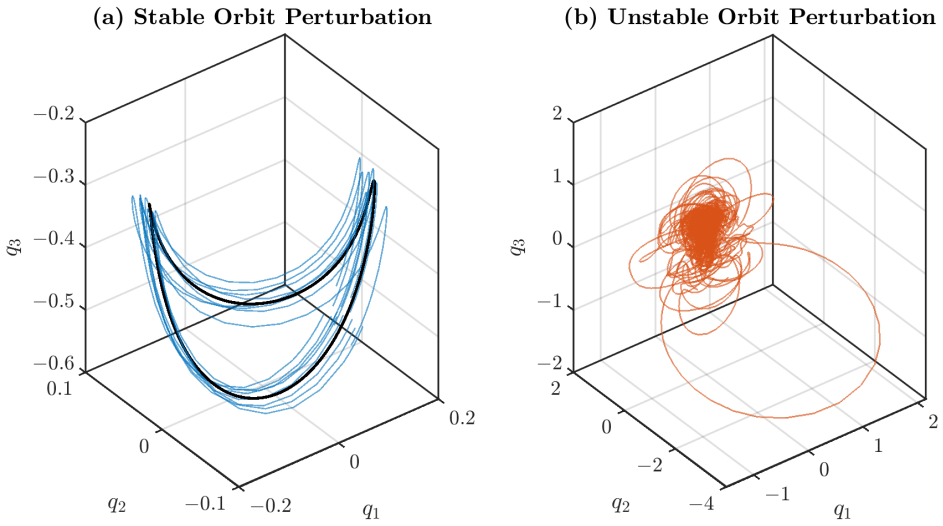


Figure 6. Time domain verification of stability. (**a**) Attraction behavior of the stable orbit (Orbit 1) subject to initial perturbations. The thick black line represents the exact reference periodic orbit (Orbit 1), while the thin blue lines denote the time-evolution trajectories starting from randomly perturbed initial states. (**b**) Repulsion and divergence behavior of the unstable orbit (Orbit 2) to initial perturbations.

5.3.3. Spectral Accuracy Convergence Comparison (Q-CSCM vs. Q-LSCM and RK Methods)

Finally, we evaluated the convergence efficiency of the Q-CSCM algorithm in solving such complex nonlinear problems and compared it against the alternative Q-LSCM baseline, the classical explicit RK4 (ERK4), and the state-of-the-art structure-preserving Gauss–Legendre implicit RK4 (GL-IRK4) methods. Using the high-precision Q-CSCM solution at $N = 100$ as the reference benchmark, we computed the initial value error $\|q_0 - q_{\text{exact}}\|$

across various degrees of freedom. For the conventional RK methods, the boundary value problem was resolved using the classical shooting method coupled with a nonlinear root-finding algorithm. In contrast, the spectral frameworks (Q-CSCM and Q-LSCM) discretize the continuous problem into a global algebraic system, allowing direct resolution via Newton–Raphson iterations.

Figure 7 shows the error convergence curves of the four methods (log-log scale). As mathematically expected, both the ERK4 and GL-IRK4 shooting methods exhibit a straight-line decline, reflecting their inherent algebraic $\mathcal{O}(h^4)$ decay rate. Although the implicit symplectic GL-IRK4 performs slightly better in error constants, it cannot escape the algebraic convergence bottleneck.

In stark contrast, both spectral collocation methods maintain a steep exponential drop, proving their spectral fidelity even for strongly nonlinear Riccati equations. More importantly, the proposed Q-CSCM (blue line) consistently yields a lower absolute error than Q-LSCM (purple line) at identical polynomial degrees. To achieve an equivalent level of accuracy, the Q-CSCM method requires at least one to two orders of magnitude fewer computational resources compared to both explicit and implicit RK shooting methods. This indicates that Q-CSCM not only preserves algebraic structure but also provides significant advantages in temporal approximation efficiency specifically for low-dimensional systems, successfully offsetting the local computational cost through massive reductions in required temporal nodes.

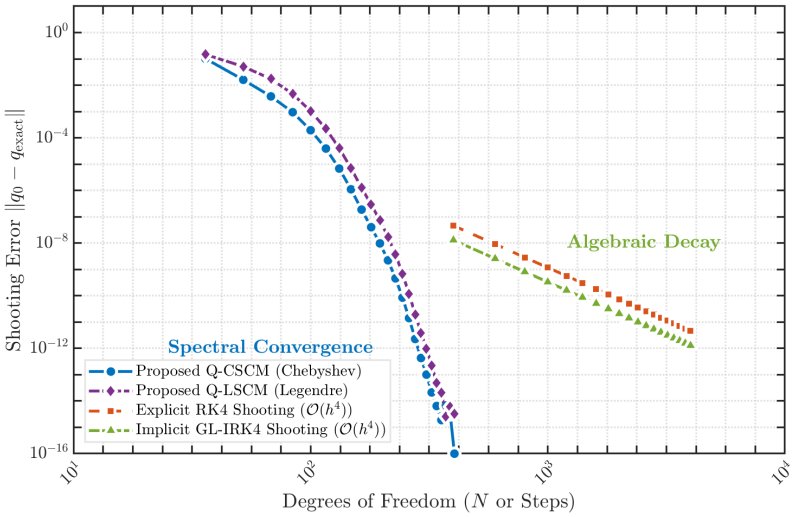


Figure 7. Convergence comparison analysis for the nonlinear Riccati oscillator. The blue solid line and purple dash-dotted line show the spectral accuracy convergence characteristic (exponential decay) of Q-CSCM and Q-LSCM, respectively, with Q-CSCM exhibiting a marginally superior error constant. The orange dashed line and green dashed–dotted line represent the algebraic convergence ($\mathcal{O}(N^{-4})$) of the explicit RK4 and implicit symplectic GL-IRK4 shooting methods. Q-CSCM achieves machine precision at extremely low degrees of freedom, exhibiting overwhelming computational efficiency over local baselines.

5.3.4. Heteroclinic Connections and Global Dynamic Structure

Besides the local stability of periodic orbits, understanding the global dynamic behavior of nonlinear systems often requires examining heteroclinic orbits connecting different invariant sets. In this section, we utilize Q-CSCM combined with numerical continuation techniques to successfully calculate the heteroclinic connection path connecting the unstable periodic orbit (Source Orbit, Orbit 2) and the stable periodic orbit (Sink Orbit, Orbit 1).

Since heteroclinic orbits are defined on the infinite time interval $(-\infty, +\infty)$, direct numerical solution faces dual challenges of truncation error and boundary condition setting. We adopt a robust continuation strategy based on Q-CSCM:

- **Step 1 Initial Value Construction:** Use the Sigmoid function to construct an initial guess path connecting Source and Sink.
- **Step 2 Time Domain Continuation:** Start from a shorter time interval $T = 1.5\pi$ and gradually increase to $T = 6.0\pi$, solving the nonlinear boundary value problem using fsolve at each step to approximate asymptotic boundary conditions.
- **Step 3 Spectral Collocation Discretization:** In each continuation step, use Q-CSCM to transform the BVP into a system of algebraic equations, ensuring high precision and numerical stability under long-time integration.

Table 4 records the numerical performance during the heteroclinic orbit continuation process. As the time span T gradually expands from 3.0π to 6.0π, the nonlinear stiffness of the problem increases significantly. However, thanks to the spectral accuracy characteristics of Q-CSCM, Newton's method maintained excellent convergence at every step. Notably, even in the final long-duration step ($T = 6.0\pi$), the algorithm could still reduce the algebraic residual to a level close to machine precision ($1.91 \times 10^{-12} \approx \sqrt{3.66 \times 10^{-24}}$) within 15 iterations, with a single-step CPU time of only 0.51 s. This ultra-high convergence accuracy, insensitive to the length of the time interval, confirms the excellent numerical robustness of the proposed algorithm in handling long-time boundary value problems of quaternion bilateral systems, overcoming the divergence problem caused by error accumulation in traditional shooting methods over long integration intervals.

Figure 8 shows the geometric structure of the calculated heteroclinic orbit in 3D phase space, depicting the heteroclinic connection path from Source to Sink. The color map represents the magnitude of the quaternion scalar part q_0, revealing the four-dimensional state evolution along the orbit. It is clearly visible in the figure that the heteroclinic orbit starts from the manifold near the unstable orbit, undergoes complex transient oscillations, and finally asymptotically converges to the stable orbit. This topological connection "from chaos to order" intuitively characterizes the global attraction basin structure of the system (The full animation of this trajectory is publicly available in our referenced GitHub repository).

Figure 9 further verifies the dynamic characteristics of the heteroclinic connection from the perspective of norm evolution. It shows that the system starts from the neighborhood of the unstable Source Orbit, exhibits a substantial transient energy amplification with the norm peaking above 1.2, before the energy monotonically dissipates and the trajectory asymptotically converges to the stable Sink Orbit. This process reveals that the heteroclinic connection is not a simple monotonic transition but involves large-amplitude nonlinear oscillations and extensive wandering in the state space.

Table 4. Convergence statistics of heteroclinic orbit numerical continuation process (Residual represents the infinity norm of the algebraic equation system $\|\mathbf{F}(\mathbf{Q})\|_\infty$).

Step	Horizon T	Iterations	Final Residual $\|\mathbf{F}(\mathbf{Q})\|_\infty$	CPU Time (s)
1	3.0π	27	3.96×10^{-13}	0.45
2	4.0π	11	7.40×10^{-10}	0.32
3	5.0π	9	4.17×10^{-13}	0.28
4	6.0π	15	1.91×10^{-12}	0.51

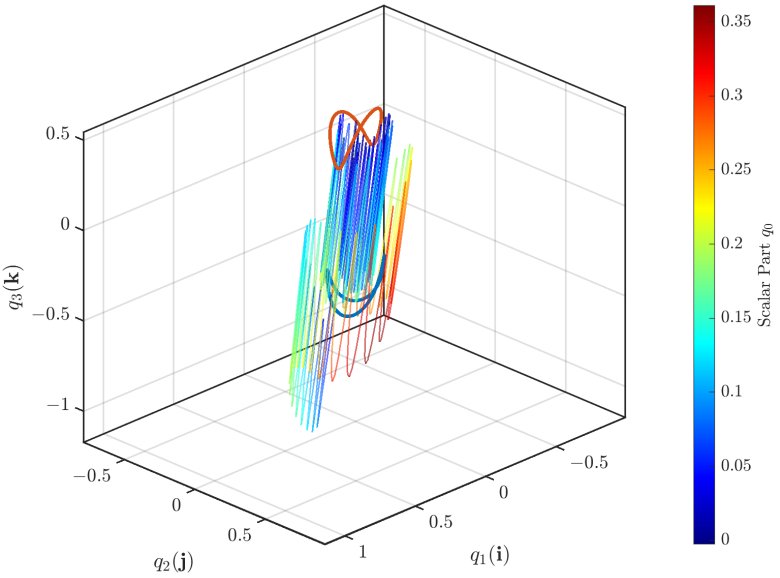


Figure 8. Phase space topology of heteroclinic connection. Heteroclinic path connecting the unstable periodic orbit (Source, red) and the stable periodic orbit (Sink, blue). Stream tube color represents the value of scalar part q_0.

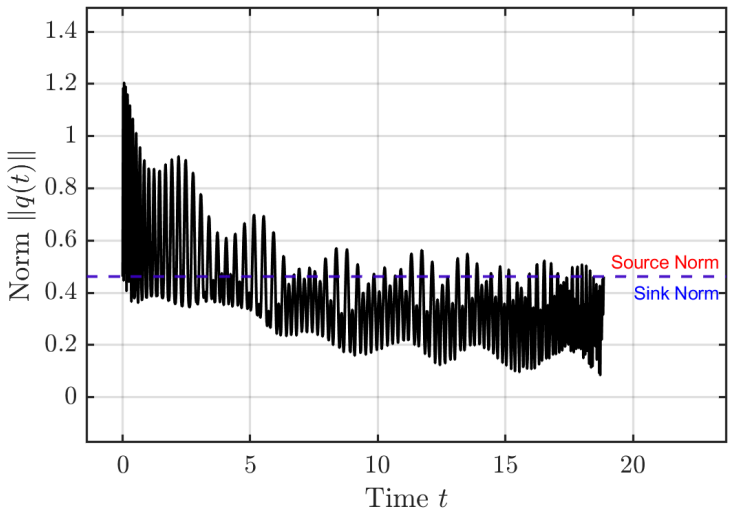


Figure 9. Norm evolution of transition dynamics. Curve of heteroclinic orbit norm $\|q(t)\|$ versus time. Red and blue dashed lines correspond to the norm levels of Source and Sink orbits respectively, showing the asymptotic transition process of the system from unstable state to stable state.

5.4. Revisiting the Classical Quaternion Riccati Equation and Dynamic Extension

For the non-autonomous quaternion Riccati equation of the following form [3]:

$$\dot{q}(t) = [q(t) - e^{\mathbf{j}t}]\mathbf{i}[q(t) + 10\mathbf{i} + e^{\mathbf{k}t}] + 1, \quad t \in [0, 2\pi]. \tag{51}$$

Wilczyński qualitatively proved that this equation has at least two 2π-periodic solutions in $\mathbb{H}$. He pointed out that one solution is asymptotically stable while the other is unstable; however, he did not provide their specific geometric forms, spatial positions, or precise convergence rates. This section reproduces them in the sense of high-precision numerical computation, combining the theoretical support of Section 3 and utilizing the Q-CSCM algorithm of Section 4.

We expand Equation (51) into the standard bilateral form $\dot{q} = qAq + Bq + qD + C$, where the coefficient mappings are equivalently transformed to

$$A(t) = \mathbf{i},\ B(t) = -e^{\mathbf{j}t}\mathbf{i},\ D(t) = \mathbf{i}(10\mathbf{i} + e^{\mathbf{k}t}),\ C(t) = 1 - e^{\mathbf{j}t}\mathbf{i}(10\mathbf{i} + e^{\mathbf{k}t}).$$

Using the Q-CSCM algorithm (with $N = 40$), we successfully converged to two distinct periodic solutions using $q \approx e^{\mathbf{j}t}$ and $q \approx -(10\mathbf{i} + e^{\mathbf{k}t})$ as initial guesses, labeled as Orbit 1 and Orbit 2 respectively. The residuals were 4.3423×10^{-12} and 1.8156×10^{-11}, and the bilateral monodromy operator spectral radii $\rho(\mathcal{M})$ for the corresponding linearized variational equations were calculated as 7.5429×10^{-8} and 1.9503×10^{27}, respectively.

Figure 10a depicts the phase portraits of these two periodic solutions within the three-dimensional imaginary subspace (q_1, q_2, q_3). Furthermore, Figure 10b illustrates the time evolution of their corresponding moduli. Figure 11 shows the local geometric details of Orbit 1 and Orbit 2.

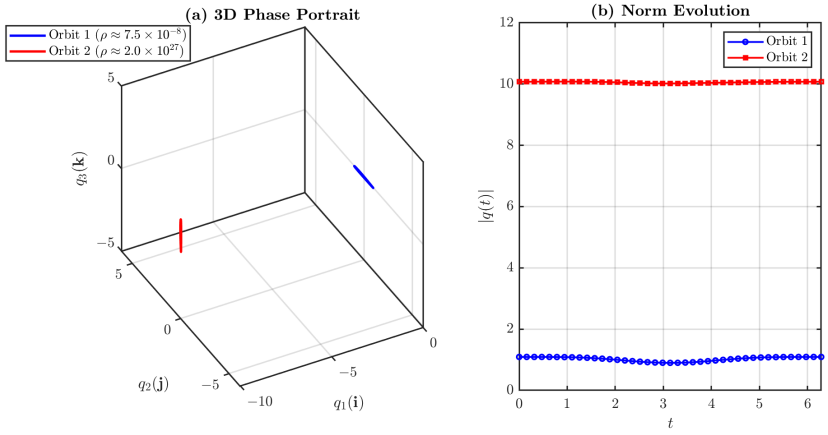


Figure 10. Numerical reconstruction of Wilczyński's benchmark problem. (**a**) Two periodic orbits in 3D phase space. Blue curve (Orbit 1) corresponds to the small amplitude solution, red curve (Orbit 2) corresponds to the large amplitude solution. (**b**) Variation of modulus of the two orbits over time, stabilizing at $\|q\| \approx 1$ and $\|q\| \approx 10$ respectively.

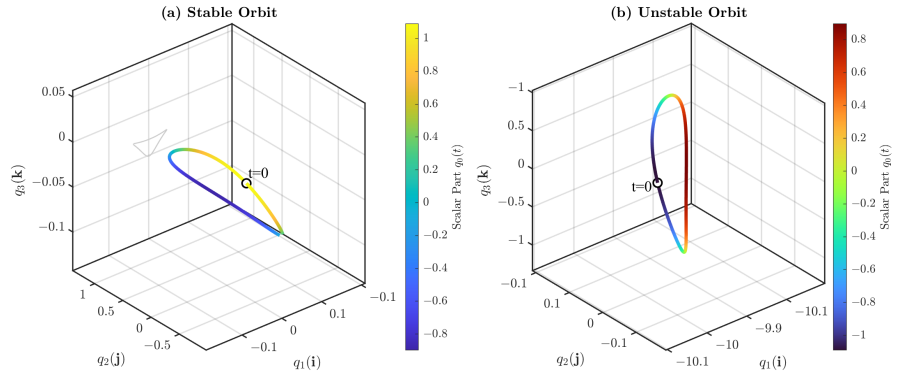


Figure 11. Spectral verification of extreme stability differences. (**a**) Local magnification of stable orbit Orbit 1; (**b**) Local magnification of unstable orbit Orbit 2. Color map represents scalar part variation.

6. Conclusions

This study demonstrates that the fundamental challenges associated with non-commutative algebras in bilateral dynamical systems can be effectively resolved by reformulating them into a structured real-valued tensor framework. By systematically extending classical real matrix theory via exact vectorization isomorphism, we reveal the tensor decoupling structure of evolution operators. The proposed "Scalar-Vector Stability Separation

Principle" serves not merely as a mathematical criterion but reveals a fundamental physical mechanism: the rotational dynamics (governed by anti-Hermitian parts) are energetically orthogonal to and independent of the dissipative evolution (governed by Hermitian parts). This perspective offers a novel theoretical framework for understanding energy conservation and dissipation in high-dimensional spin systems and rigid body attitude control.

Furthermore, the discovery of the cubic scaling law ($\varepsilon_0 \propto \beta^3$) relating the robustness threshold to the spectral gap suggests an inherent sensitivity of bilateral systems near critical stability points. Unlike traditional qualitative Lyapunov methods, this algebraic criterion provides a quantitative boundary for parameter design in engineering applications, ensuring structural stability even under slowly varying perturbations.

Numerically, it is imperative to draw a strict distinction between the theoretical analytical decoupling and the actual computational cost of the numerical solver. While the Q-CSCM algorithm demonstrates superior temporal spectral accuracy and structure-preserving properties for stiff Riccati oscillators ($n = 1$), its algorithmic reliance on dense global matrix inversion ($\mathcal{O}(n^6N^3)$) imposes severe spatial dimensionality bottlenecks. The practical efficiency of the current Q-CSCM is thus primarily temporal and strictly localized to low-dimensional regimes ($n = 1$). Future research will focus on reconciling this tension by bypassing the dense Jacobian inversion through the integration of matrix-free Newton–Krylov iterative solvers (such as GMRES), extending this operator-theoretic framework to spatially high-dimensional quaternion partial differential equations, and exploring tailored geometric integrators.

Author Contributions: Conceptualization, X.S.; methodology, X.S.; software, X.S.; formal analysis, X.S.; writing—original draft preparation, X.S.; writing—review and editing, J.Z.; supervision, J.Z.; funding acquisition, J.Z. All authors have read and agreed to the published version of the manuscript.

Funding: This work was supported by the Yunnan Fundamental Research Projects [grant numbers 202401AS070148, 202401AT070570] and the Scientific Research Funds of the Educational Department of Yunnan Province [grant number 2024J0030].

Data Availability Statement: The MATLAB (version R2023b) source code for the algorithms and numerical experiments presented in this paper is publicly available on GitHub. at: https://github.com/happy-rabbit123/Q-CSCM-Algorithm.git (accessed on 24 March 2026).

Conflicts of Interest: The authors declare that they have no known competing financial interests or personal relationships that could have appeared to influence the work reported in this paper. The funders had no role in the design of the study; in the collection, analyses, or interpretation of data; in the writing of the manuscript; or in the decision to publish the results.

References

1. Kuipers, J.B. *Quaternions and Rotation Sequences: A Primer with Applications to Orbits, Aerospace and Virtual Reality*; Princeton University Press: Princeton, NJ, USA, 1999; p. 394.
2. Adler, S.L. *Quaternionic Quantum Mechanics and Quantum Fields*; International Series of Monographs on Physics; Oxford University Press: Oxford, UK, 1995; p. 608.
3. Wilczyński, P. Quaternionic-valued ordinary differential equations. The Riccati equation. *J. Differ. Equ.* **2009**, *247*, 2163–2187. [CrossRef]
4. Wilczyński, P. Quaternionic-valued ordinary differential equations II. Coinciding sectors. *J. Differ. Equ.* **2012**, *252*, 4503–4528. [CrossRef]
5. Gasull, A.; Llibre, J.; Zhang, X. One-dimensional quaternion homogeneous polynomial differential equations. *J. Math. Phys.* **2009**, *50*, 082705. [CrossRef]
6. Alesker, S. Quaternionic Monge-Ampère equations. *J. Geom. Anal.* **2003**, *13*, 205–238. [CrossRef]
7. Abreu Blaya, R.; Bory Reyes, J.; Guzmán Adán, A.; Schneider, B. Boundary value problems for the Cimmino system via quaternionic analysis. *Appl. Math. Comput.* **2012**, *219*, 3872–3881. [CrossRef]

8. Zhu, L.; Cong, E.y.; Zhang, X. Global exponential stability conditions for quaternion-valued neural networks with leakage, transmission and distribution delays. *AIMS Math.* **2023**, *8*, 19018–19038. [CrossRef]
9. Lv, J.; Wang, J.; Liu, R. Hyers-Ulam Stability of Linear Quaternion-Valued Differential Equations. *Electron. J. Differ. Equ.* **2023**, *2023*, 1–15. [CrossRef]
10. Kou, K.I.; Xia, Y.H. Linear Quaternion Differential Equations: Basic Theory and Fundamental Results. *Stud. Appl. Math.* **2018**, *141*, 3–45. [CrossRef]
11. De Leo, S.; Ducati, G.C. Solving simple quaternionic differential equations. *J. Math. Phys.* **2003**, *44*, 2224–2233. [CrossRef]
12. Hairer, E.; Lubich, C.; Wanner, G. *Geometric Numerical Integration: Structure-Preserving Algorithms for Ordinary Differential Equations*; Springer Science & Business Media: Berlin/Heidelberg, Germany, 2006; Volume 31. [CrossRef]
13. Blanes, S.; Casas, F. *A Concise Introduction to Geometric Numerical Integration*; Monographs and Research Notes in Mathematics; Chapman and Hall/CRC: Boca Raton, FL, USA, 2016.
14. Jia, Z.; Ng, M.K. Structure Preserving Quaternion Generalized Minimal Residual Method. *SIAM J. Matrix Anal. Appl.* **2021**, *42*, 616–634. [CrossRef]
15. Li, T.; Wang, Q.W. Structure Preserving Quaternion Biconjugate Gradient Method. *SIAM J. Matrix Anal. Appl.* **2024**, *45*, 306–326. [CrossRef]
16. Ding, W.; Liu, Z.; Li, Y.; Wei, A.; Zhang, M. New structure-preserving algorithms of Gauss-Seidel and successive over-relaxation iteration methods for quaternion linear systems. *Numer. Algorithms* **2024**, *95*, 1309–1323. [CrossRef]
17. Zhang, F. Quaternions and matrices of quaternions. *Linear Algebra Its Appl.* **1997**, *251*, 21–57. [CrossRef]
18. So, W. Quaternionic Left Eigenvalue Problem. *Southeast Asian Bull. Math.* **2005**, *29*, 555–564.
19. Brenner, J.L. Matrices of quaternions. *Pac. J. Math.* **1951**, *1*, 329–335. [CrossRef]
20. Rodman, L. *Topics in Quaternion Linear Algebra*; Princeton Series in Applied Mathematics; Princeton University Press: Princeton, NJ, USA, 2014; p. 384.
21. Higham, N.J. *Functions of Matrices*; Society for Industrial and Applied Mathematics: Philadelphia, PA, USA, 2008. [CrossRef]
22. Hetmaniok, E.; Słota, D.; Szczygieł, M.; Pleszczyński, M.; Wituła, R. Hermite-Bell's Polynomials for Negative Powers. In Proceedings of the 2019 Applications of Electromagnetics in Modern Engineering and Medicine (PTZE), Janow Podlaski, Poland, 9–12 June 2019; pp. 56–59. [CrossRef]
23. Kato, T. *Perturbation Theory for Linear Operators*, 2nd ed.; Classics in Mathematics; Originally published as volume 132 in the series: Grundlehren der mathematischen Wissenschaften; Springer: Berlin/Heidelberg, Germany, 1995; pp. XXI, 623. [CrossRef]
24. Kato, T. On the Adiabatic Theorem of Quantum Mechanics. *J. Phys. Soc. Jpn.* **1950**, *5*, 435–439. [CrossRef]
25. Coppel, W.A. *Dichotomies in Stability Theory*; Lecture Notes in Mathematics; Springer: Berlin/Heidelberg, Germany, 1978; Volume 629. [CrossRef]
26. Daleckii, J.L.; Krein, M.G. *Stability of Solutions of Differential Equations in Banach Space*; Translations of Mathematical Monographs; American Mathematical Society: Providence, RI, USA, 1974; Volume 43, p. 386.
27. Sacker, R.J.; Sell, G.R. A spectral theory for linear differential systems. *J. Differ. Equ.* **1978**, *27*, 320–358. [CrossRef]
28. Gottlieb, D.; Orszag, S.A. *Numerical Analysis of Spectral Methods: Theory and Applications*; CBMS-NSF Regional Conference Series in Applied Mathematics; Society for Industrial and Applied Mathematics: Philadelphia, PA, USA, 1977; Volume 26. [CrossRef]
29. Shen, J.; Tang, T.; Wang, L.L. *Spectral Methods: Algorithms, Analysis and Applications*, 1st ed.; Springer Series in Computational Mathematics; Springer: Berlin/Heidelberg, Germany, 2011; pp. XVI, 472. [CrossRef]
30. Canuto, C.; Hussaini, M.Y.; Quarteroni, A.; Zang, T.A. *Spectral Methods: Fundamentals in Single Domains*, 1st ed.; Scientific Computation; Springer: Berlin/Heidelberg, Germany, 2006; pp. XXII, 563. [CrossRef]
31. Hetmaniok, E.; Pleszczyński, M.; Słota, D.; Wituła, R. On similarities between exponential polynomials and Hermite polynomials. *J. Appl. Math. Comput. Mech.* **2013**, *12*, 93–104. [CrossRef]
32. Trefethen, L.N. *Spectral Methods in MATLAB*, 1st ed.; Software, Environments, and Tools; Society for Industrial and Applied Mathematics: Philadelphia, PA, USA, 2000; pp. xviii, 165. [CrossRef]
33. Boyd, J.P. *Chebyshev and Fourier Spectral Methods*, 2nd ed.; Dover Publications: Mineola, NY, USA, 2001.

Disclaimer/Publisher's Note: The statements, opinions and data contained in all publications are solely those of the individual author(s) and contributor(s) and not of MDPI and/or the editor(s). MDPI and/or the editor(s) disclaim responsibility for any injury to people or property resulting from any ideas, methods, instructions or products referred to in the content.